ANNUAL REVIEWS Further
Click here to view this article's online features:
- Download figures as PPT slides
- Navigate linked references
- Download citations
- Explore related articles
- Search keywords

Applications of Surface Second Harmonic Generation in Biological Sensing

Renee J. Tran, Krystal L. Sly, and John C. Conboy

Department of Chemistry, University of Utah, Salt Lake City, Utah 84112;
email: conboy@chem.utah.edu

Annu. Rev. Anal. Chem. 2017. 10:387–414

First published as a Review in Advance on March 16, 2017

The *Annual Review of Analytical Chemistry* is online at anchem.annualreviews.org

https://doi.org/10.1146/annurev-anchem-071015-041453

Copyright © 2017 by Annual Reviews.
All rights reserved

Keywords

second harmonic generation, biosensors, lipid membranes, spectroscopy, surfaces, chirality, proteins, small molecules

Abstract

Surface second harmonic generation (SHG) is a coherent, nonlinear optical technique that is well suited for investigations of biomolecular interactions at interfaces. SHG is surface specific due to the intrinsic symmetry constraints on the nonlinear process, providing a distinct analytical advantage over linear spectroscopic methods, such as fluorescence and UV-Visible absorbance spectroscopies. SHG has the ability to detect low concentrations of analytes, such as proteins, peptides, and small molecules, due to its high sensitivity, and the second harmonic response can be enhanced through the use of target molecules that are resonant with the incident (ω) and/or second harmonic (2ω) frequencies. This review describes the theoretical background of SHG, and then it discusses its sensitivity, limit of detection, and the implementation of the method. It also encompasses the applications of surface SHG directed at the study of protein-surface, small-molecule–surface, and nanoparticle-membrane interactions, as well as molecular chirality, imaging, and immunoassays. The versatility, high sensitivity, and surface specificity of SHG show great potential for developments in biosensors and bioassays.

INTRODUCTION

With the increased use of biosensors and bioassays, understanding biomolecular interactions at surfaces has become increasingly important. The initiation of many critical biochemical processes in vitro also occurs at surfaces, particularly lipid membranes. These processes include the release of neurotransmitters and hormones upon the binding of G-coupled proteins with their lipid membrane–incorporated receptors, (1, 2), invagination of bacteria toxins and viruses upon attachment of viral and bacterial proteins to glycolipids and/or glycoproteins within the membrane (3, 4), and recognition of an antibody by a lipid membrane–incorporated antigen (5, 6). The complex surface chemistry and biomolecular interactions at interfaces are crucial to a host of biosensor platforms, such as biotinylated monolayers, nanoparticle-labeled antibodies, and biopolymer conjugated microspheres used in chemical sensing (7–9). The need for analytical tools that are capable of quantifying biomolecular interactions at interfaces with high sensitivity is therefore of great clinical and biochemical importance.

Recently, there has been an effort to develop label-free methods, such as surface plasmon resonance (SPR) and quartz-crystal microbalance (QCM), for the investigation of biological surface interactions (7, 10–13). However, both SPR and QCM require large molecular analytes (>10 kDa) to produce a detectable mass change at the surface, meaning that detecting low molecular weight molecules, peptides, and small proteins is nearly impossible. A few signal enhancement methods have proven successful in overcoming this limitation. One such method involves adsorbing bovine serum albumin (BSA) to the surface followed by adsorption of the small-molecule analyte (14, 15). Despite the advancements in label-free methods, no distinct front-runner has surpassed the sensitivity of fluorescence and ease of use of methods such as enzyme-linked immunosorbent assay (ELISA).

One label-free technique that has shown incredible promise in providing the sensitivity of fluorescence is the nonlinear optical method of second harmonic generation (SHG). Although SHG has been employed since the early 1980s in the surface characterization of a variety of interfaces, such as those used in photovoltaics (16) and thin film chemistry (17), only relatively recently has it been applied as a method for investigating biomolecular interactions at interfaces (18–21). Eisenthal and coworkers have made some noteworthy advances using SHG as a biomolecular detection method at lipid membranes. These include determining the orientation of adsorbed dye molecules to a lipid bilayer (22), investigating the surface potential of liposomes composed of negatively charged lipids (23, 24), examining the transport kinetics of dye molecules across a liposome (24–27), and monitoring the binding of peptides and proteins at a lipid membrane surface (28, 29). SHG is also successful in monitoring the real-time molecular transport across a membrane (27, 30). In addition, second harmonic (SH) scattering is used to measure the interfacial response of liposomes and nanoparticles in solution and to obtain insight on molecular kinetics and distribution at surfaces (31–33). In most of these SHG studies, dye molecules were used as probes to monitor the various properties of adsorption, transport, and orientation of molecular species associated with lipid membranes (22, 23, 25, 26, 34). More recently, SHG studies demonstrated molecular interactions with membranes in which the inherent optical properties of the biomolecules themselves were used to generate the SH response, producing a truly label-free technique (19, 20, 35). Even with long data acquisition times for monitoring steady-state binding and the use of dye molecule probes, SHG has some clear advantages over the more common label-free techniques of SPR and QCM. Most notably, its extreme surface specificity, high sensitivity, and insensitivity to randomly ordered nonspecific adsorption make SHG a viable label-free alternative capable of providing limits of detection (LOD) similar to those seen in the fluorescence methods.

In this review, we discuss the advantages of surface SHG as a detection method for simple and complex biomolecular interactions at interfaces. SHG has the versatility to detect both large protein/peptide molecules and small-molecule interactions without the use of probes or labels. Applications of SHG for the investigation of protein, small-molecule, and nanoparticle interactions with biological membranes using imaging and correlation analysis are also discussed, further illustrating the potential versatility and application of SHG as a label-free detection method in biological sensing.

SURFACE SECOND HARMONIC GENERATION

SHG is a coherent second-order nonlinear optical technique that is inherently surface specific and possesses the spectroscopic characteristics of UV-Visible (UV-Vis) absorbance spectroscopy. Because the theory of SHG was described in detail and reviewed in several publications (36, 37), this review focuses on the general principles of SHG, such as surface specificity, resonant enhancement, and sensitivity, which make it a valuable label-free detection method for quantifying the interaction of biological species at interfaces. SHG is produced when two incident beams of the same frequency (ω) are spatially and temporally overlapped to produce an output of twice the frequency (2ω) (**Figure 1**). The output is governed by the induced nonlinear polarization

$$P_i^{(2)}(2\omega) = \chi_{ijk}^{(2)} E_j E_k, \qquad 1.$$

where $\chi_{ijk}^{(2)}$ is the second-order susceptibility tensor that characterizes the interactions of the two incoming electric fields, E_j and E_k, with the molecules at the surface to produce an output SH field, E_i. The subscripts of $\chi_{ijk}^{(2)}$ can take on any of the Cartesian coordinates, x, y, and z. Due to the symmetry constraints of $\chi_{ijk}^{(2)}$, the SH response is only produced in noncentrosymmetric media. Biomolecules such as collagen that are noncentrosymmetric were studied extensively in SHG microscopy (38–40). However, there is no SH response seen in bulk isotropic phases, but an SH response is produced at an interface between isotropic materials where the inversion symmetry of the bulk is broken. This property makes SHG extremely surface specific, eliminating any contributions from bulk species and making it highly sensitive to adsorbed molecules at an interface. It is the unique surface specificity of SHG for which the technique is known (41–50),

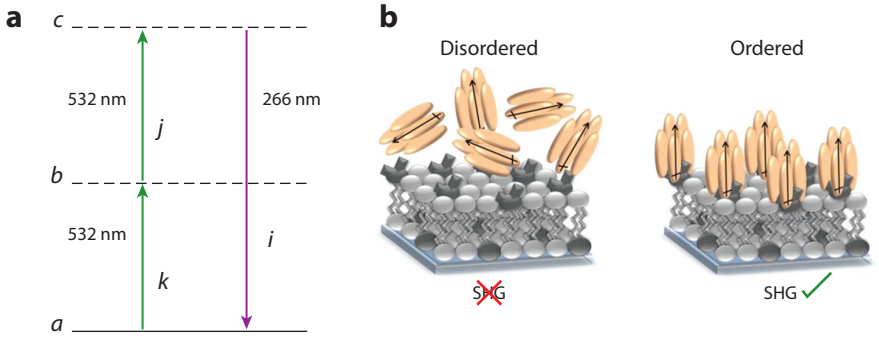

Figure 1

(*a*) Energy diagram depicting the surface second harmonic generation (SHG) process with a, b, and c representing the initial, intermediate, and final states, respectively, and i, j, k representing the output and two input fields. In this case, the inputs are at 532 nm, whereas the output is at 266 nm. (*b*) The schematic depicts the break in inversion symmetry and ordered molecular orientation required for a second harmonic response to be produced.

and this review focuses on the use of surface SHG in particular and its applications in biological sensing.

Sensitivity

The SHG intensity is proportional to the square of $\chi^{(2)}_{ijk}$, the macroscopic second-order susceptibility tensor, which consists of both a nonresonant portion, $\chi^{(2)}_{NR}$, and a resonant portion, $\chi^{(2)}_{R}$:

$$I_{SHG} \propto \left|\chi^{(2)}_{ijk}\right|^2 \propto \left|\chi^{(2)}_{NR} + \chi^{(2)}_{R}\right|^2. \quad 2.$$

At the interface between two dielectric media under resonant conditions, $\chi^{(2)}_{NR}$ is usually quite small in comparison to $\chi^{(2)}_{R}$. The resonant susceptibility term is expressed as

$$\left(\chi^{(2)}_{ijk}\right)_R \propto N \sum_{a,b,c} \frac{\langle a|\mu_i|c\rangle \langle a|\mu_j|b\rangle \langle b|\mu_k|c\rangle}{(2\hbar\omega - E_{ca} - i\Gamma_{ca})(\hbar\omega - E_{bc} - i\Gamma_{bc})}, \quad 3.$$

where N is the surface density of molecules, $\hbar$ is Planck's constant, μ is the Cartesian coordinate dipole operator, Γ is the transition line width, and a, b, and c represent the initial, intermediate, and final electronic states, respectively, of the molecular species of interest, depicted in **Figure 1**. Several important properties that affect the sensitivity of SHG for adsorbed molecules at an interface are exemplified in Equation 3. First, $\chi^{(2)}_{R}$ is proportional to the number density (N) of molecules at the surface, resulting in an N^2 dependence on the measured SHG intensity. Second, if the energy of the incident or SH fields is resonant with an electronic transition of the molecules at the interface, an increase in the numerator and decrease in the denominator of Equation 3 results in an increase of the resonant susceptibility and subsequent SH intensity. These first two properties impart a well-defined correlation between the measured response and the concentration of species being interrogated and a frequency dependence of that response. Third, the sensitivity of SHG is also dictated by the orientational average of the molecules at the surface, as indicated by the brackets in the numerator of Equation 3 that represent the average over all dipole orientations of the adsorbed molecules for a specific electronic transition. When the net dipole orientation of the molecules is anisotropic or highly ordered, there is an increase in $\chi^{(2)}_{R}$ and the overall SHG response. As most binding interactions of biomolecules to interfaces of both technological and biochemical interest occur in a highly ordered orientation, there is a significant increase in the SHG response upon binding. When the net dipole orientation of the molecules at the surface is isotropic in nature, which is usually the case with random, nonspecific adsorption, $\chi^{(2)}_{R}$ is negligible, and there is a minimal SHG response. This dependence of SHG on the net orientation of the surface-adsorbed species makes it extremely well suited for measuring specific biomolecular interactions at interfaces. Thus, the surface specificity and sensitivity only to specific adsorption events provide SHG with a clear advantage over fluorescence, SPR, and QCM.

Limit of Detection

Resonant enhancement substantially increases the sensitivity of SHG and lowers its LOD to a submonolayer of molecules at the surface. In the studies conducted by the authors and other examples presented in this review, the incident frequency is typically set in the visible or near-infrared (IR) region, with the SHG in the UV or visible region of the spectrum. These wavelengths are particularly well suited to probe molecules with a double bond or π-conjugated system. Most small molecules, metabolites, and nucleotides contain π electrons, providing the opportunity for a resonantly enhanced SHG response. Additionally, the amino acid residues tryptophan, tyrosine,

and phenylalanine all have aromatic rings, in addition to the amide backbone which has a strong n-π^* transition, allowing resonant enhancement in the SHG response when detecting proteins and peptides. Shorter wavelength resonances (<260 nm) might seem better suited for SHG detection, but the lack of suitable optical filters for these wavelengths severely compromises detection and subsequently the sensitivity and LOD.

Unlike SPR and QCM, which struggle to detect low molecular weight species with high sensitivity, SHG is able to detect these species with LOD down to fg/cm^2 (35, 51). **Table 1** shows a comparison of the LOD for several molecules detected via SPR, fluorescence, ELISA, and SHG. The sensitivity of SHG is substantially better than that of the label-free techniques of SPR and QCM, as well as that of enzyme-based amplification methods such as ELISA. Though SPR appears to have higher sensitivity and LOD for the detection of streptavidin, this is misleading, as localized enhancement of the surface was used by employing silver nanoparticles (52). In addition to demonstrating lower LOD and greater versatility in the types of molecular species which can be detected with SHG, all of this was achieved without use of spectroscopic labels.

Implementation

SHG can be performed in either a copropagating or counterpropagating fashion, with each implementation having its own advantages and disadvantages. Optical densities for generating efficient SHG are usually in the MW/cm^2 range; thus, pulsed laser sources are employed. Depending on the pulse duration, pulse energies range from several nanojoules to microjoules per pulse for femtosecond lasers and millijoules per pulse for nanosecond lasers. For short laser pulses (femtoseconds and picoseconds), the incident laser is usually focused to achieve the needed field intensities at the surface, whereas for nanosecond lasers, much larger illumination can be used. The repetition rate of the laser is also important to consider for signal averaging; however, potential laser damage to the sample must also be considered at high repetition rates. Detection is usually accomplished with a charge-coupled device, photomultiplier tube, or avalanche photodiode due to the low conversion efficiency of SHG, which is typically on the order of 1×10^{-6} to 1×10^{-4} (SHG photons out/photons in), depending on the optical geometry (external versus internal reflection) (53, 54) and sample being investigated.

In the copropagating geometry (**Figure 2*a***), the two electric fields originate from the same input beam, which is from either a femtosecond, picosecond, or nanosecond coherent laser source, and the SH emission is detected along the same optical path. By carefully choosing the input and output polarization combinations, the complete set of surface susceptibility elements ($\chi^{(2)}_{zzz}$, $\chi^{(2)}_{izi}$, $\chi^{(2)}_{zii}$, where i can be x or y) can be retrieved (55). In addition to quantifying the surface density of adsorbates, the molecular orientation of adsorbates can also be obtained if a single strong dipole transition exists in the molecule, denoted by $\alpha^{(2)}_{g,zzz}$, by taking the ratio of intensities of the 45°-in/s-out and p-in/p-out polarization combinations (where s is perpendicular to the plane of incidence and p is parallel to the plane of incidence), using the following equations (56):

$$I_{2\omega}^{\text{in/out}}(t<0) \propto |AN_g(t<0)\alpha^{(2)}_{g,zzz}\left(\langle\cos\theta\rangle_{\rho_g(\theta,t<0)} - c\langle\cos^3\theta\rangle_{\rho_g(\theta,t<0)}\right)|^2, \quad 4a.$$

$$R(t=0) = \frac{\langle\cos^3\theta\rangle_{\rho_g(\theta,t<0)}}{\langle\cos^5\theta\rangle_{\rho_g(\theta,t<0)}}, \quad 4b.$$

$$\rho = \frac{1}{\sqrt{2\pi\sigma^2}}\exp\left[-\frac{(\theta-\theta_0)^2}{2\sigma^2}\right], \quad 4c.$$

Table 1 Comparison of the limit of detection for surface second harmonic generation (SHG), surface plasmon resonance (SPR), fluorescence, and enzyme-linked immunosorbent assay (ELISA) for several small molecules and proteins

Analyte	SHG		SPR		Fluorescence		ELISA	
	fM	pg/cm^2	fM	pg/cm^2	fM	pg/cm^2	fM	pg/cm^2
Ibuprofen	227.3 ± 0.1	46.9 ± 4.7	415 (138)	95 (138)	ND	ND	ND	ND
Tetracaine	441.4 ± 41.2	116.7 ± 10.9	835 (138)	1,918 (138)	ND	ND	5,900,000 (139)	1,562,000 (139)
SBN	0.040 ± 0.001	114 ± 4	415 (138)	95 (138)	ND	ND	ND	ND
Tolnaftate	4,251.0 ± 172	1,306.8 ± 52.8	2,025,075 (138)	623,723 (138)	ND	ND	ND	ND
Azithromycin	4.8 ± 0.4	3.6 ± 0.3	533 (138)	405 (138)	ND	ND	ND	ND
Streptavidin	84 ± 17	4,413 ± 883	0.06 (52)	3 (52)	433 (64)	22,872 (64)	ND	ND
Cholera toxin B	0.7 ± 0.1	44.6 ± 6.6	7 (52)	393 (52)	5 (140)	285 (140)	3 (141)	195 (141)
Avidin	80.1 ± 0.3	5,280 ± 17	0.06 (52)	4 (52)	433 (64)	28,578 (64)	ND	ND
Peanut agglutinin	40.3 ± 3.7	4,433 ± 407	50,169 (142)	5,511,000 (142)	1,562 (143)	171,784 (143)	ND	ND
Antibiotin	17 ± 0.9	2,384 ± 119	50,169 (142)	7,023,660 (142)	3 (143)	429 (143)	0.005 (144)	0.5 (144)

Abbreviations: fM, femtomolar concentration; ND, no data; SBN, S-(+)-1,1′-bi-2-naphthol.

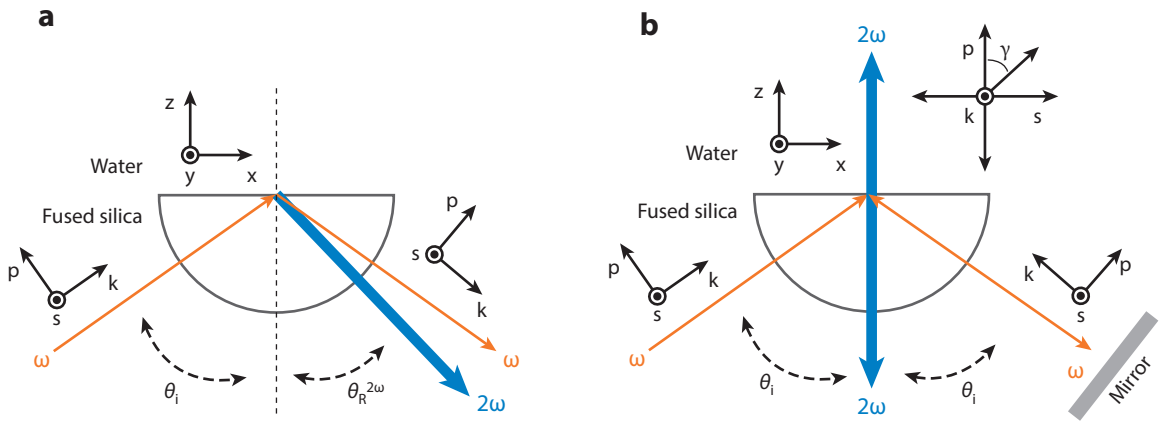

Figure 2

(*a*) Copropagating and (*b*) counterpropagating second harmonic geometry at the interface between silica and water. Circles indicate vectors coming out of the plane, where x, y, and z define the interfacial coordinate system. ω is the frequency of the two inputs and 2ω is the frequency of the output. (*b*, *upper right*) γ is defined in the beam coordinate system, where p is parallel to the plane of incidence, s is perpendicular to the plane of incidence, and k indicates direction of propagation. Figure adapted with permission from Reference 55 and the Optical Society.

where $I_{2\omega}^{\text{in/out}}$ is the general formula for the SHG intensity, with A and c being functions of the incident and outgoing angles with respect to the surface normal, θ being tilt angle from the surface normal, N_g being the number of ground state molecules at the surface, and $\alpha_{g,zzz}^{(2)}$ being the molecular hyperpolarizability. Local field factors are related to the dielectric constants of the fundamental and SH frequencies in the bulk media and molecular layer. R is the order parameter, and ρ is the orientational distribution function, where θ_0 is the mean orientational angle.

An alternative optical configuration, which the authors have developed, is to use a counterpropagating beam geometry in which the two electric fields originate from opposite sides of the surface normal, which is illustrated in **Figure 2*b***. For this optical arrangement, the xz plane is defined as the plane of incidence and z is the surface normal. This approach limits the accessible surface susceptibility elements to $\chi_{izi}^{(2)}$ and $\chi_{xyz}^{(2)}$ when chiral species are present, which means that the orientation of analytes cannot be determined directly as with the copropagation geometry. However, this approach has the advantage of a significant gain in sensitivity due to the detection geometry, as the generated SH field is emitted along the surface normal that is spatially separated from the incident excitation source (~67° compared to ~4° in copropagating SHG). Counterpropagation also allows for direct detection of the chiral and achiral susceptibilities by measuring the SH intensity for orthogonal polarization states of the SHG emission, as discussed in more detail below. Applications of both the co- and counterpropagating optical geometries for measuring a variety of biological interactions at interfaces are summarized in the following sections.

APPLICATIONS OF SURFACE SECOND HARMONIC GENERATION

Quantifying Protein–Surface Interactions

The binding of proteins to surfaces and surface-bound ligands is responsible for a host of biological functions. Understanding and quantifying these surface interactions elucidate important biochemical events on cell surfaces and provide insight for better bioassay design and

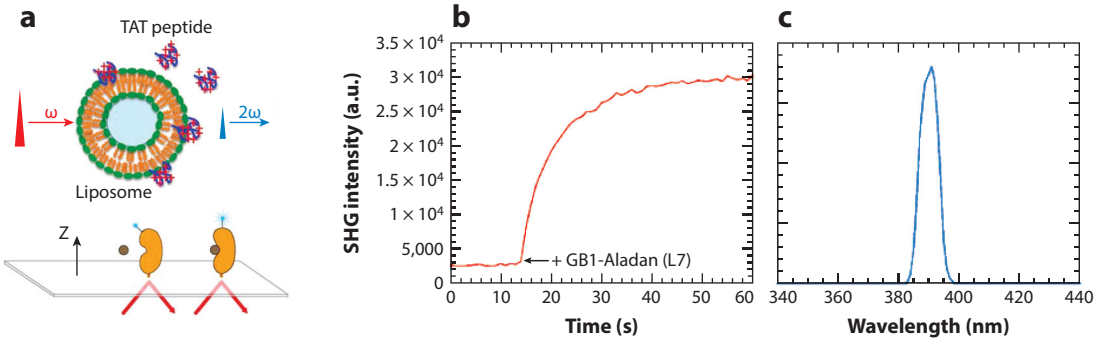

Figure 3

Schematics of different SHG investigations into protein interactions. (*a*) TAT peptides binding to the surface of liposomes composed of DOPC or DOPG with the input at ω (800 nm), the output at 2ω (400 nm), and labeled protein bound to a surface while incident laser light strikes the surface, creating an evanescent wave. Panel adapted with permission from Reference 57. Copyright 2014, National Academy of Sciences. Signal intensity depends on the average orientation of the label relative to the normal (z-axis) and a conformational change alters the orientation, resulting in a signal change (*b*,*c*). (*b*) SHG intensity as a function of time of the adsorption of GB1-Aladan to a glass coverslip. (*c*) SHG intensity as a function of wavelength of the adsorbed protein. Panels *b* and *c* adapted with permission from Reference 63. Copyright 2008, American Chemical Society. Abbreviations: DOPC, 1,2-dioleoyl-*sn*-glycero-3-phosphocholine; DOPG, 1,2-dioleoyl-*sn*-glycero-3-phospho(1′-rac-glycerol); SHG, surface second harmonic generation; TAT, transacting activator of transduction.

development. SHG is a valuable technique for characterizing such protein–surface interactions. Typically, the binding properties of proteins are measured by obtaining a binding isotherm where the SHG intensity is collected as a function of the bulk analyte concentration. The binding isotherm can be used to evaluate the binding affinity by fitting the data to a particular binding model. The most commonly used binding model is the Langmuir isotherm, which for SHG is expressed as (35)

$$I_{\mathrm{SHG}} \propto \left(\frac{\sqrt{I_{\mathrm{SHG}}^{\mathrm{max}}} K_0 [c]}{1 + K_0 [c]} \right)^2, \qquad 5.$$

where $I_{\mathrm{SHG}}^{\mathrm{max}}$ is the SH intensity at saturation of binding sites, [*c*] is the concentration of the analyte, and K_0 is the binding affinity. This model is adequate for simple monovalent interactions, as it assumes that there are negligible protein–protein or ligand–ligand interactions.

Several groups have used SHG for the investigation of a variety of protein–surface interactions. For example, SHG was utilized to investigate the binding of the transacting activator of transduction (TAT) protein (**Figure 3**), which is integral to the progression of AIDS, to liposomes composed of 1-palmitoyl-2-oleoyl-*sn*-glycero-3-phosphocholine (POPC) or 1-palmitoyl-2-oleoyl-*sn*-glycero-3-phospho-(1′-rac-glycerol) (POPG) (57). This study found a decrease in SH intensity in relation to an increased positive surface potential of the membrane, due to the binding of the TAT protein. In their study, Rao and coworkers (57) were able to obtain the binding affinity and maximum number of TAT proteins that bound to the liposomes using SHG. Matar et al. (58) studied the adsorption of tryptophan-rich peptides to lipid monolayers containing 1,2-dipalmitoyl-*sn*-glycero-3-phosphocholine (DPPC) or 1,2-dipalmitoyl-*sn*-glycero-3-phospho-(1′-rac-glycerol) (DPPG) spread at the air–water interface using SHG. The SH intensity was collected as a function of the incident polarization. This procedure allowed the quantification of the adsorbed peptide, as well as observation of an oriented monolayer of peptide through examination of the polarization dependent SHG response, where the SHG intensity as a function of polarization angle (γ) was

expressed as

$$I^{\text{p-out}} = |a\cos^2\gamma + b\sin^2\gamma|^2, \quad 6a.$$

$$I^{\text{s-out}} = |c\,\sin 2\gamma|^2, \quad 6b.$$

with a, b, and c being parameters that depend on geometric configuration, the refractive indices of air, and aqueous phase at the input and output wavelengths, and the nonvanishing independent tensor elements of the interface (58). There was a general increase in the a, b, and c parameters observed with adsorption of peptide, but the tilt angle was not reported. These studies demonstrate some of the capabilities of SHG to explore protein–membrane interactions and to obtain both binding data and structural information on protein orientation at the membrane interface.

Other studies have coupled SH active dye molecules with proteins that are weakly SH active to observe the adsorption and orientation of proteins at interfaces. Eckenrode & Dai (59) coupled polylysines (consisting of 14 or 75 amino acid units) with the chromophore malachite green to measure binding at the surface of microparticles. The solution of polystyrene microparticles was pumped with a liquid jet in front of the 844 nm incident beam from a Ti:sapphire laser. The polylysines were titrated into the particle solution, where the SH intensity was measured as a function of concentration. This study was able to determine the surface density of the polylysines adsorbed on the polystyrene particles (59). In a study by Salafsky (60), maltose-binding protein was coupled with [1-(3-(succinimidyloxycarbonyl)benzyl)-4-(5-(4-methoxyphenyl)oxazol-2-yl)pyridinium bromide succimidyl] (PyMPO) and spread at the air–water interface in a Langmuir trough. Using an incident beam at 800 nm from an argon–ion laser, the resulting electric field amplitude with increasing concentration of the protein–dye conjugate was obtained and is shown in **Figure 3**, where the orientation of the adsorbed maltose-binding protein at the air–water interface was also determined and found to be $27° \pm 3°$ with respect to the surface normal (z-axis of the protein) (60).

SHG can also reveal conformational changes of proteins in addition to surface density and orientation. In a study by Moree et al. (61), maltose-binding protein, calmodulin, and *Escherichia coli* dihydrofolate reductase (DHFR) were allowed to adsorb to lipid bilayers that had formed in wells on a glass slide. The SH response was recorded as maltose or lactose added to the wells containing maltose-binding protein, calmodulin-binding peptide was added to wells containing calmodulin, and methotrexate or trimethoprim was added to the wells containing DHFR. The conformational changes of these proteins induced by their ligands, including amino acid rotation and protein domain motion, were detected by SHG. Moree et al. (62) also hypothesized that modulating the conformation of α-synuclein (a protein thought to be related to the progression of Parkinson's disease) would affect aggregation of the protein in cells. They investigated this hypothesis by labeling α-synuclein with SHG2-maleimide dye before allowing the labeled protein to adsorb to the surface wells on a glass slide (62). The adsorbed protein was then incubated with the ligand BIOD303 (a pharmacophore from the Maybridge fragment library). BIOD303 was found to only bind a specific conformation of α-synuclein, which showcased the ability of SHG to detect specific conformations of proteins. Another molecule that can be used to enhance SH signal is the unnatural amino acid Aladan. Salafsky & Cohen (63) wanted to investigate the structure of a globular immunoglobulin–binding protein (GB1), and labeled GB1 by incorporating Aladan into the B1 domain. GB1–Aladan complexes were then immobilized onto the surface of glass coverslips. When an immunoglobulin G Fc fragment was allowed to interact with the GB1–Aladan complex, a change in conformation of the protein was observed using SHG. The various studies summarized above demonstrate the capability of SHG to detect protein conformational changes.

More complex protein binding interactions were also investigated via SHG. For example, a detailed study of the binding of avidin and its two analogs, streptavidin and neutrAvidin, to biotin-conjugated lipids in a 1,2-dioleoyl-*sn*-glycero-3-phosphocholine (DOPC) lipid bilayer was performed via SHG (35). The binding of these proteins to the biotin–membrane surface demonstrated cooperative binding interactions. **Figure 4** shows the binding isotherm of avidin binding to a biotinylated DOPC lipid bilayer with the data fit to both the Langmuir binding model and the cooperativity binding model. It is clear that the avidin–biotin interaction is best described using the cooperativity model ($R_2 = 0.9993$) developed by Zhao and coworkers (64), which is described as

$$I_{\mathrm{SHG}} \propto \left\{ \frac{\sqrt{I_{\mathrm{SHG}}^{\max}}\omega^{\left(\sqrt{I_{\mathrm{SHG}}}/\sqrt{I_{\mathrm{SHG}}^{\max}}\right)} K_0 [P]}{1 + \omega^{\left(\sqrt{I_{\mathrm{SHG}}}/\sqrt{I_{\mathrm{SHG}}^{\max}}\right)} K_0 [P]} \right\}^2 . \quad 7.$$

Assuming that avidin binds biotin in a square lattice, then $\omega = \eta^4$. A negative cooperativity results when $\eta < 1$ and the protein–protein interaction reduces the ligand–protein binding. Positive cooperation occurs when $\eta > 1$ and the protein–protein interaction increases the ligand–protein binding, with the cooperativity model reducing to the Langmuir model when $\eta = 1$. It is important to note that the protein–protein cooperative behavior is most apparent at very low nanomolar concentrations of avidin as indicated by the sigmoidal shape at the low concentration end of the isotherm. This is most likely why studies of avidin–biotin binding using SPR have failed to report this cooperative behavior, but SHG was able to detect the cooperativity of the avidin molecules due to its high sensitivity (64).

SHG is also able to detect multivalent protein–ligand interactions, which can be described by the Hill-Waud model (65):

$$I_{\mathrm{SHG}} \propto \left(\frac{\sqrt{I_{\mathrm{SHG}}^{\max}} K_a^n [c]^n}{1 + K_a^n [c]^n} \right)^2 , \quad 8.$$

where n is the Hill coefficient used to describe the affinity of the protein for its ligand once another ligand is already bound. Cholera toxin B (CTb) binding to monosialotetrahexosylganglioside (GM_1) measured by SHG was best described by the Hill-Waud model due to the cooperativity between the ligands binding to the CTb pentamer. The CTb–GM_1 interaction showed a positive interaction, suggesting that once one ligand is bound to CTb, there is an increase in the binding of another ligand (66). Again, the signature cooperative sigmoidal shape at low CTb concentrations is apparent, illustrating the importance of high sensitivity and low LOD for measuring such protein–ligand interactions, which is possible via SHG.

Another study investigating the interaction between the protein peanut agglutinin (PnA) and GM_1 doped in a DOPC bilayer more dramatically demonstrates the importance of detecting low surface densities of proteins. One of the few studies looking at the binding properties of this complex was performed by QCM and reported a binding affinity determined using the Langmuir binding model (12). Performing a similar binding experiment using SHG, a study determined that PnA binds to GM_1 and experiences electrostatic repulsion between the negatively charged PnA molecules (pI $\sim$ 6) at pH 7.4 (67). **Figure 4** illustrates the binding behavior of PnA to GM_1 and the data fit to the Frumkin model, which for SHG is expressed as (18, 66)

$$I_{\mathrm{SHG}} \propto \left\{ \frac{\sqrt{I_{\mathrm{SHG}}^{\max}} K_a [P] \exp\left(2g\sqrt{I_{\mathrm{SHG}}}/RT\right)}{1 + K_a [P] \exp\left(2g\sqrt{I_{\mathrm{SHG}}}/RT\right)} \right\}^2 . \quad 9.$$

The g coefficient describes the electrostatic interactions between the charged protein molecules on the surface, where $g < 0$ indicates a repulsive electrostatic interaction between protein molecules,

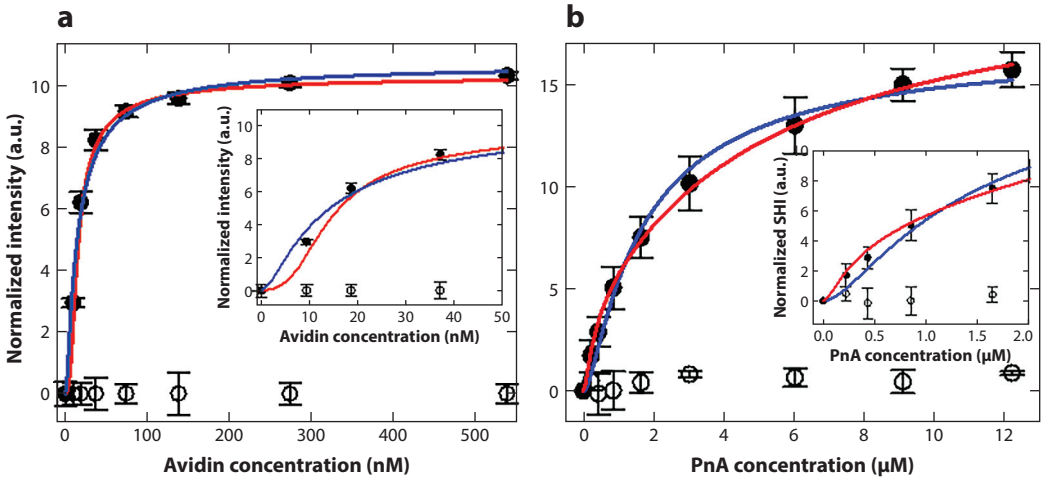

Figure 4

(*a*) SHG intensity versus bulk avidin concentration for avidin binding to a DOPC bilayer containing 4 mol% biotin-cap-DOPE (*black circles*) and 0 mol% biotin-cap-DOPE (*white circles*). Lines represent the fit to the cooperativity binding model (*red*) and the Langmuir model (*blue*). The error bars represent the standard deviation from three independent experiments. The inset zooms in on the low avidin concentrations to better show the separation of the two fits. Panel adapted with permission from Reference 35. Copyright 2012, American Chemical Society. (*b*) SHG versus bulk PnA concentration binding to 5 mol% GM_1 doped into a DOPC bilayer recorded at steady-state equilibrium (*black circles*) and binding to a pure DOPC bilayer (*white circles*). Lines represent the fits to the Frumkin binding model (*red*) and Langmuir model (*blue*). The error bars represent the standard deviation from three independent experiments. The inset zooms in on the low PnA concentrations to better show the separation of the two fits. Panel adapted with permission from Reference 66. Copyright 2014, American Chemical Society. Abbreviations: DOPC, 1,2-dioleoyl-*sn*-glycero-3-phosphocholine; DOPE, 1,2-dioleoyl-*sn*-glycero-3-phosphoethanolamine; GM_1, monosialotetrahexosylganglioside; PnA, peanut agglutinin; SHG, surface second harmonic generation.

and $g > 0$ indicates an attractive electrostatic protein–protein interaction (35). For PnA binding to GM_1, there was a strong repulsive electrostatic interaction between the negatively charged PnA molecules. A fit to the Frumkin model led to a binding affinity six times greater than that obtained by Jansoff and coworkers using the Langmuir model (66). Part of the discrepancy between the binding affinities obtained from the data in **Figure 4** using SHG and those obtained using QCM is due to the QCM data not being collected under a steady-state condition, making the reported binding affinity mass transport limited and artificially lower. In addition to emphasizing the importance of maintaining steady-state equilibria, this study elegantly demonstrates the tremendous importance of having high sensitivity capable of detecting low analyte concentrations to determine the cooperative and electrostatic behavior of the analyte/ligand molecules. The high surface specificity and high sensitivity of SHG shown in **Figure 4** allow SHG to detect the presence of both protein–protein and protein–ligand cooperative behavior, making the reported binding kinetics and thermodynamics more precise and informative.

Detecting Biomolecular Interactions Using Chirality

In addition to detecting the surface interactions of proteins with incredible sensitivity and minimal nonspecific adsorption contributions, as shown in the previous section, the intrinsic symmetry constraints of SHG allow for the detection of molecular chirality at surfaces. Most biological molecules, including proteins and DNA, possess intrinsic chirality arising from the secondary and tertiary structures of these macromolecules (68). These structures could in principle be used as

spectroscopic markers for the detection of surface-adsorbed species based on their chiral nature. Nonlinear optical spectroscopy was first used to detect chirality in 1967 (69, 70). It has since been demonstrated that linearly polarized light can detect chirality in ordered multilayer films (71–73). More recently, SHG was coupled with circular dichroism (CD) and optical rotary dispersion (ORD) to create a surface-sensitive analog of linear CD and ORD spectroscopy (74–79).

The chiral SHG of two SH active bacteriorhodopsin films on opposite sides of the same substrate was demonstrated by Yamada et al. (80). Glass slides were dipped into purple membrane (bacteriorhodopsin) solution to form bacteriorhodopsin thin films. An SH signal from the film was measured in four polarization combinations (p-p, s-p, p-s, s-s, for polarizer and analyzer) while rotating the sample. They found that the interference fringes in the p-p and s-p polarizations had almost an opposite phase compared to p-s, attributed to the difference for the transformation between achiral and chiral components. Another study utilized the chiral response from L-cysteine and D-cysteine that were adsorbed onto the surface of silver nanoparticles (81). SHG was used to measure the optical nonlinearity of the system and the enantiomers were found to have opposite responses at 45° and −45° output polarizations. This result was attributed to the chiral nature of the molecules, as the bare silver nanoparticles had the same response at both polarizations.

As mentioned previously, counterpropagating measurements do not rely on the phase difference between the chiral and achiral tensors, allowing for the direct detection of chirality based on light emission. Specifically, Kriech & Conboy (82) used counterpropagating SHG to investigate the interaction of melittin, a hemolytic peptide isolated from bee venom, with a POPC planar-supported lipid bilayer (PSLB). Melittin exists as a disordered random coil in an aqueous solution. When intercalated into a membrane, melittin undergoes a structural change to form a well-ordered amphipathic α-helix due to hydrophobic interactions with the membrane (83). Although a myriad of techniques have investigated the orientation of melittin upon binding to a membrane, including attenuated total reflection infrared spectroscopy (ATR-IR) (84), NMR spectroscopy (85, 86), and oriented CD (87–89), most of these methods lack the sensitivity to investigate the orientation of melittin using a single lipid bilayer. This forces multilayers of lipids to be used, which decreases the biorelevancy of these models. Using SHG to collect binding isotherms for the achiral and chiral SH emission, it was possible to determine the percent change in the α-helical structure of melittin as a function of surface coverage (82). SHG revealed that, as the surface coverage of melittin increased, so did the α-helical order of the peptide. This was the first application of SHG used to monitor the binding of a peptide to a lipid bilayer using the secondary structure of the molecule as a probe (82). Additionally, SHG was able to monitor the role of the enzyme phospholipase A_2 (PLA_2) on the orientation of melittin association in a membrane (82). **Figure 5** illustrates the significant role that PLA_2 has on orienting melittin upon binding to the lipid bilayer. Although it was previously shown that melittin first binds parallel to the membrane, this study was the first to determine the perpendicular orientation of melittin after the cleavage of the phosphate headgroups by PLA_2, primarily due to the higher sensitivity of SHG over other methods (82). These studies showcase the use of SHG for the detection of protein adsorption in biological systems and the analysis of protein interfacial phenomena (90, 91).

Small-Molecule–Surface Interactions

Similar to the study of protein–surface interactions, dye molecules are used to probe membrane surface properties via SHG. Salafsky & Eisenthal (22) measured the adsorption of the dye PyMPO to a 4:1 DOPC:DOPG [1,2-dioleoyl-*sn*-glycero-3-phosphocholine:1,2-dioleoyl-*sn*-glycero-3-phospho(1′-rac-glycerol)] bilayer doped with 1 mol% Texas Red. PyMPO was found to adsorb to the outer leaflet of the bilayer and was unable to cross the bilayer. The adsorption of

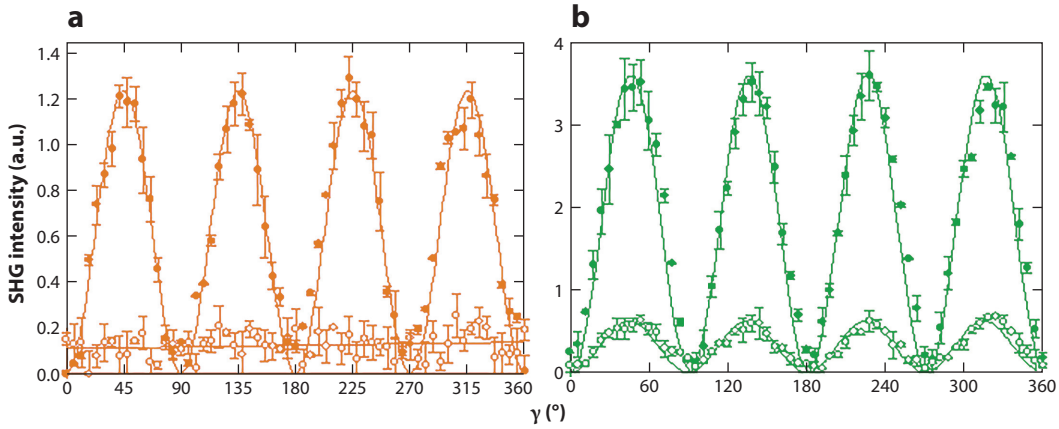

Figure 5

(*a*) SHG intensity as a function of polarization angle for a POPC membrane with synthetic melittin for the chiral (*open orange circles*) and achiral (*solid orange circles*) responses. (*b*) SHG intensity as a function of polarization angle for a POPC membrane with melittin and PLA_2 for the chiral (*open green circles*) and achiral (*solid green circles*) responses. Figure adapted with permission from Reference 82. Abbreviations: PLA_2, phospholipase A_2; POPC, 1-palmitoyl-2-oleoyl-*sn*-glycero-3-phosphocholine; SHG, surface second harmonic generation.

malachite green to POPC liposomes containing different percentages of POPG was measured by injecting the liposomes into a malachite green solution (23). An initial increase in SH intensity was due to adsorption to the outer surface of the liposome (**Figure 6**), whereas the subsequent decay in intensity was attributed to diffusion of malachite green across the bilayer and adsorption to the inner surface of the membrane. This study found that the adsorption and transport of malachite green were linearly dependent on the concentration of DOPG, but not DOPC, which meant that

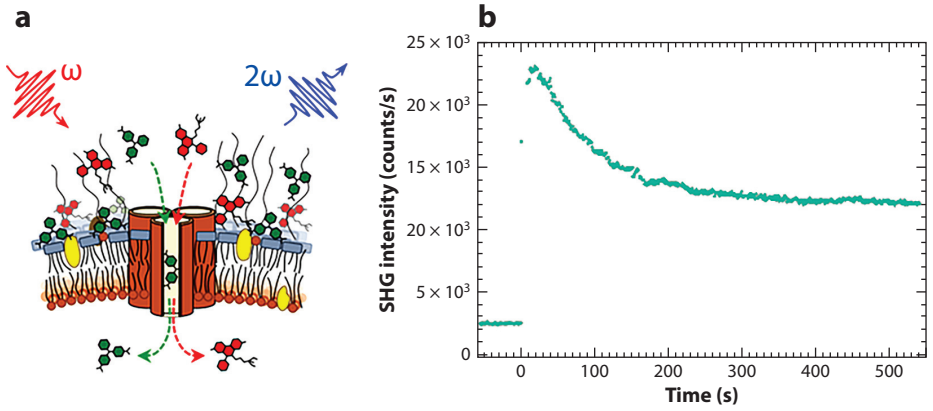

Figure 6

(*a*) Graphic representation of the initial MG adsorption to the surface of the membrane and transportation through the membrane. (*b*) SHG decay curve upon injection of liposome into an MG solution. The concentrations of POPG and MG were 13 μM and 2 μM, respectively, after mixing. Incident light was at 832 nm, whereas the signal was recorded at 416 nm. Dots represent data points for 1 s of integration time. Figure adapted with permission from References 24 and 92. Copyright 2016, American Chemical Society. Abbreviations: MG, malachite green; POPG, 1-palmitoyl-2-oleoyl-*sn*-glycero-3-phospho-(1′-rac-glyerol); SHG, surface second harmonic generation.

a larger negative charge was ideal for malachite green adsorption. This study was expanded upon by investigation of the transport kinetics of the malachite green cation (MG^+) across DOPG bilayers when gramicidin A (an ion channel), valinomycin (an alkali ion carrier), and carbonyl cyanide-m-chlorophenylhydrazone (CCCP, a proton transporter) were present in the membrane (27). The presence of gramicidin A resulted in the largest decrease in SH signal. However, it was confirmed that MG^+ did not block the gramicidin A channel, but it reached the same steady-state value regardless of when gramicidin A was added. When valinomycin was added, the decay in SH signal was attributed to the exchange of MG^+ into the liposome as valinomycin transported out the sodium cations. CCCP was found to have negligible effect on the transport of MG^+, as the signal in its presence was similar to the signal when no transporters were present.

In a similar study by Hai-Lung Dai's group (27), the transport of MG^+ through an *E. coli* membrane was measured using SHG. MG^+ was added to the cell suspension, and the initial adsorption of MG^+ to the outer membrane was observed with a sharp rise in SH signal, much like the study from Eisenthal's group (23). The transport through the outer membrane appeared to be faster than transport through the inner membrane. Dai's group (92) built on these results by studying the transport of propidium, a weakly SHG active molecule, coupled with malachite green across the *E. coli* membranes. The reduction of the maximum signal and the decay rate indicated competition between malachite green and propidium for transport through the outer membrane. This demonstrated that, although propidium is only weakly SHG active, the transport rate could still be obtained. In another study, Nguyen et al. (18) used UV-Vis SFG, a variant of SHG, to detect the association of ibuprofen, azithromycin, tolnaftate, and tetracaine to DOPC bilayers. The equilibrium association constants, surface densities, and LOD of these drugs were obtained in this study, along with correlating the membrane specificity with octanol–water partition coefficients. A study by Mitchell (93) monitored the adsorption of indole to a DPPC monolayer at the air–water interface, using a monolayer of the chromophore hexadecyl 3-indoleacetate as a reference for a known surface density. In the absence of DPPC, there was no adsorption of indole to the monolayer, which revealed specificity of indole for the lipid monolayer. This was significant, as the specificity of drugs for their targets determines their effectiveness and overall bioavailability.

The interaction of the selective estrogen receptor modulators, raloxifene, tamoxifen, and three tamoxifen metabolites (4-hydroxytamoxifen, *N*-desmethyltamoxifen, and endoxifen) with lipid bilayers was investigated by the authors' group (19) (**Figure 7**). These molecules play a significant role in the inhibition of estrogen-induced breast tumor proliferation. At clinically relevant concentrations of these drugs, there was a higher affinity to liquid phase lipid membranes than bilayers in a mixed liquid and gel phase coexistence. These molecules did not adsorb to gel phase lipids at all, which was due to the tighter packing of the membrane. More importantly, these studies indicated a direct connection between the clinical activities of the drugs with their affinity for fluid phase lipid membranes, showing that their activity is controlled in large part by the bioavailability of the drugs.

Surface Second Harmonic Imaging

The previous sections focused on using SH spectroscopy for investigating individual protein or small-molecule interactions. Joining SHG with imaging provides a powerful combination capable of spatially resolving such interactions. The first coupling of SHG and imaging was demonstrated in 1974 when Hellwarth and Christensen combined SHG with an optical microscope (94). SHG imaging has since been used to investigate a myriad of surfaces, including the uniformity of the interfacial region of a metalloporphyrin film (95), the carrier motion at interfaces of organic devices (96), and the chirality of surface immobilized small molecules (97). Several groups have employed

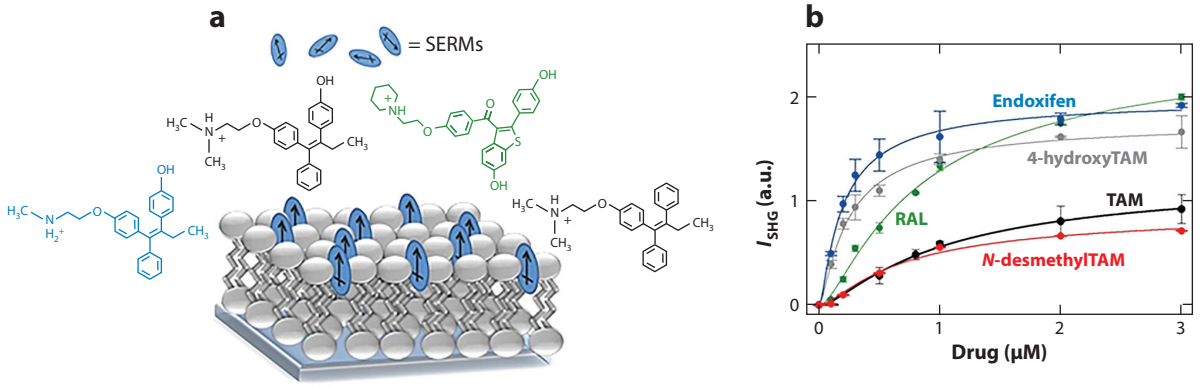

Figure 7

(*a*) Graphic representation of the SERMs as blue disks binding to a lipid membrane supported on a substrate. (*b*) Adsorption isotherms for the SERMs binding to a DOPC bilayer. Solid lines are fits to the Langmuir model. Figure adapted with permission from Reference 19. Copyright 2014, American Chemical Society. Abbreviations: DOPC, 1,2-dioleoyl-*sn*-glycero-3-phosphocholine; RAL, raloxifene; SERM, selective estrogen receptor modulator; SHG, second harmonic generation; TAM, tamoxifen.

SHG imaging to examine biological tissues; however, these studies rely on the bulk structural symmetry of proteins in tissue and cells to generate the SHG signal. For example, Macias-Romero et al. (98) used SHG to image barium titanate nanoparticles and optimize an SHG microscope configuration, then used the optimized configuration to image living neurons. The use of surface SHG imaging to examine biological interfaces is mainly limited to using SHG-active dye molecules as probes to investigate membrane potential (99, 100), individual liposomes (101), and kinetic transport (102, 103). Other studies have used gold nanoparticles as labels to investigate membrane proteins with SHG imaging as a way to detect single molecules (104). More recently, the authors investigated drug–lipid interactions at a liquid/solid interface in a high-throughput manner using label-free SHG imaging (20). The SHG images of the small-molecule drug tetracaine binding to a multicomponent lipid bilayer array are shown in **Figure 8**. This study provides important insights on the role of bulk drug concentration, lipid phase, temperature, and cholesterol on drug–lipid membrane interactions simultaneously. It was also the first study to utilize SHG imaging without the use of label to investigate surface biomolecular interactions in a high-throughput manner and showcase the ability to directly image the association of a small-molecule drug into a multicomponent lipid microarray with high sensitivity.

In addition to the ability of SHG imaging to directly image surface biomolecular interactions, the authors demonstrated that the spatially and temporally coherent SH output and plane-wave nature of surface SHG eliminated the need for a lens system (105). Removing the lens system simplifies detection, increases photon collection efficiency, lowers optical aberrations, and increases the detection area. SHG lensless images of a patterned DOPC bilayer containing S-(+)-1,1′-bi-2-naphthol (SBN) were collected. The results from the images collected for different sized line widths at multiple detector-sample distances demonstrate the incredible spatially and temporally coherent output of SHG. The SHG lensless imaging system was able to readily resolve line widths down to 223 μm at a detector-sample distance of 7.6 cm and line widths of 397 μm up to a detector-sample distance of ∼30 cm. This study was the first of its kind, thoroughly investigating the SH output beam propagation and its coherence. It is important to note that SHG lensless imaging is only possible in the counterpropagating geometry, as the SH output is emitted normal to the surface without any instantaneous distortion in the wavefront from emission at an angle

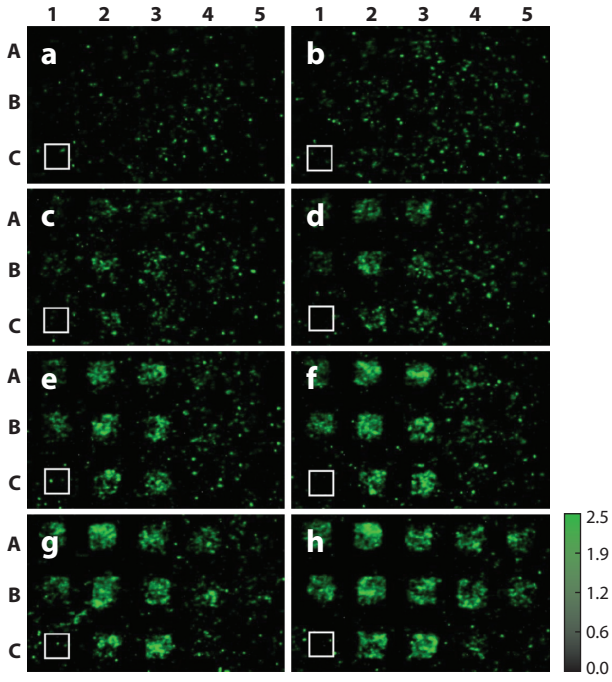

Figure 8

The normalized SHG images of tetracaine binding to a multicomponent lipid bilayer array containing the following lipid compositions: DOPC (1A, 1B, 2A, 2B); no lipids, control spot (1C) labeled by the white box; DOPC + 28 mol% cholesterol (2C); SOPC (3A, 3B); SOPC + 28 mol% cholesterol (3C); DMPC (4A, 4B); DMPC + 28 mol% cholesterol (4C); DPPC (5A, 5B); DPPC + 28 mol% cholesterol (5C). Each image represents a different bulk tetracaine concentration: 0 mM (*a*); 0.05 mM (*b*); 0.11 mM (*c*); 0.21 mM (*d*); 0.42 mM (*e*); 0.83 mM (*f*); 1.59 mM (*g*); and 3.32 mM (*h*). The images were collected at 27°C. Each bilayer patch is approximately 400 × 400 μm. Figure adapted with permission from Reference 20. Copyright 2011, American Chemical Society. Abbreviations: DOPC, 1,2-dioleoyl-*sn*-glycero-3-phosphocholine; DMPC, 1,2-dimyristoyl-*sn*-glycero-3-phosphocholine; DPPC, 1,2-dipalmitoyl-*sn*-glycero-3-phosphocholine; SHG, surface second harmonic generation; SOPC, 1-stearoyl-2-oleoyl-*sn*-glycero-3-phosphocholine.

(51, 97). In the field of biosensors and medical diagnostics, SHG lensless imaging could be extremely advantageous, as it is capable of directly imaging and analyzing larger arrays without a label.

As described earlier, chirality can be detected using SHG. Not surprisingly, the direct optical imaging of chirality originating from a planar surface film has proven to be extremely challenging due to the limited optical path length, small change in relative absorbance (between left and right circularly polarized light), and the physical limitation of the optics in conventional microscopes, which prevent their use in the UV. Using SHG's inherent surface sensitivity and its ability to discriminate between the symmetry of surface-adsorbed species, in combination with the counterpropagating optical geometry discussed above, the first optical image originating solely from the intrinsic chirality of a surface film was obtained.

The intrinsic chiralities of the enantiomers of 1,1′-bi-2-naphthol (RBN and SBN) were used to image a patterned PSLB on a silica substrate using counterpropagating SHG and a modified Olympus microscope (97). Kriech and colleagues used a polydimethylsiloxane stamp to create a series of alternating holes in a fluid PSLB by microcontact printing (μCP). Solutions of RBN, SBN, and a racemic mixture of RBN and SBN were injected above the μCP PSLB to obtain an

image. The bright regions in the SHG image correspond to regions in which RBN (or SBN) has intercalated in the membrane, whereas the dark regions correspond to voids in the lipid film that have been removed by μCP. Because RBN does not bind to bare silica, no chiral emission is observed. RBN and SBN exchange freely between solution and a lipid membrane, allowing for easy substitution of enantiomers. To demonstrate that the SHG imaging technique is sensitive to the chiral species at the surface, a racemic mixture of RBN and SBN was also injected above the membrane surface. Because equal numbers of each enantiomer were bound within the membrane, the net result was no SHG emission. SHG imaging introduces the possibility of directly observing protein domains in cell membranes and chiral structures in monolayer films. SHG imaging also has an advantage over conventional fluorescence microscopy by using the intrinsic chirality of a target molecule as a probe instead of a fluorescent tag.

Nanoparticle–Membrane Interactions

Biomolecular interactions at an interface can also be probed by SHG using functionalized nanoparticles. Troiano et al. (106) used SHG to investigate the interactions of gold nanoparticles with lipid bilayers formed on silica substrates. The gold nanoparticles were functionalized with negatively or positively charged groups, mercaptopropionic acid (MPA) or polyelectrolyte poly(allylamine)hydrochloride (PAH), respectively. The adsorption to bilayers composed of DOPC, 1,2-dimyristoyl-*sn*-glycero-3-phosphocholine (DMPC), 1,2-dimyristoyl-*sn*-glycero-3-phospho-(1-rac-glycerol) (DMPG), and 1,2-dioleoyl-3-trimethylammonium-propane (DOTAP) was measured, as shown in **Figure 9**. The differently charged groups on the nanoparticles exhibited different effects on the extent of nanoparticle adsorption to the bilayers. There was more surface coverage for the PAH functionalized nanoparticles, but they were found to be limited by charge–charge repulsion and ionic strength. Though there was a lower surface density of MPA-functionalized nanoparticles, the SH signal was larger, which was attributed to constructive interference. The ability of SHG to measure the interaction of these gold nanoparticles with

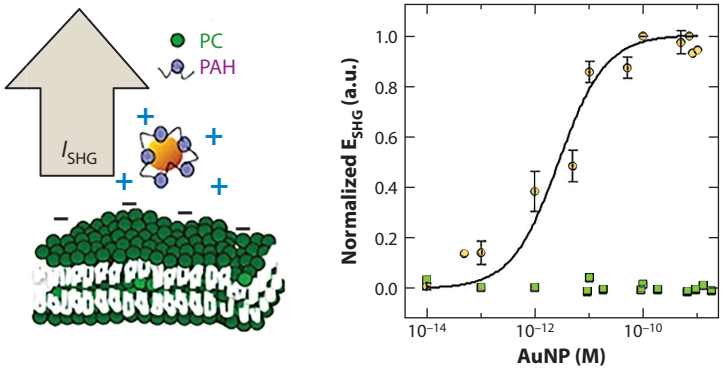

Figure 9

Normalized SHG electric field as a function of nanoparticle concentration after the addition of 4-nm gold nanoparticles (*yellow circles*) to supported lipid bilayers composed of 9:1 DOPC:DOTAP. Green squares represent results using fused silica with no bilayer present, and the solid line represents a fit to the Langmuir model. Figure adapted with permission from Reference 106. Copyright 2016, American Chemical Society. Abbreviations: AuNP, gold nanoparticle; DOPC, 1,2-dioleoyl-*sn*-glycero-3-phosphocholine; DOTAP, 1,2-dioleoyl-3-trimethylammonium-propane; PAH, poly(allylamine hydrochloride); PC, phosphocholine; SHG, surface second harmonic generation.

membranes can be further developed to investigate other biological systems with functionalized nanoparticles.

Protein–Protein, DNA–DNA, Protein–DNA, and Small-Molecule–DNA Interactions

In addition to membrane interactions, protein–protein, protein–DNA, and small-molecule–DNA interactions have also been investigated by SHG. Perrenoud-Rinuy et al. (107) examined the adsorption of the proteins myoglobin and hemoglobin along with the chromophore Fe(III) protoporphyrin IX (PpIX) at a 1,2-dichloroethane and buffer interface, which acts as a model membrane. This study determined the Gibbs free energy of adsorption for each protein, and the adsorption isotherms revealed that both myoglobin and hemoglobin exhibited protein–protein interactions upon adsorption. This result provides insight on what interactions will be present during adsorption of these proteins to an in vitro membrane. Similarly, characterization of DNA interactions can be measured by immobilizing DNA strands on a substrate. Kumal et al. (108) used SHG to investigate the photo-activated release of microRNA (miRNA) immobilized on silver nanoparticles. The incident beam of 800 nm was directed at the functionalized nanoparticles in a cuvette, and the SH response was measured as a function of time. The SH intensity was attributed to the negatively charged nucleotides, and a decay in intensity after irradiation was thought to be a result of the cleaving of miRNA from the nanoparticle surface. The bare silver nanoparticles had the same signal as the minimum of the time-dependent response, which indicated complete cleaving of the miRNA. In a separate study, Walter & Geiger (109) covalently attached single-stranded and double-stranded DNA (dsDNA) to fused silica substrates and were able to calculate the number density of DNA on the surface. Doughty et al. (110) applied this technique to investigate protein–DNA interactions by immobilizing a 90-base-pair DNA duplex containing the recognition sequence for *E. coli* restriction enzyme (EcoR1) to polystyrene microparticles. EcoR1 specifically cleaves the duplex between G and A in the recognition sequence, causing a 74-base-pair fragment to go into free solution, which is thought to cause a decrease in SH intensity. After injection of EcoR1 over the particles, an initial jump in intensity was attributed to the binding of EcoR1 to the DNA. After the initial jump, the SH intensity decayed, which was attributed to the cleaving of DNA by EcoR1. SHG could detect the specificity of EcoR1 for its recognition sequence. This ability could be utilized for targeting other proteins using their recognition sequences in DNA functionalized surfaces.

Investigation of the drugs developed for their anticancer abilities with DNA is especially desired. The binding of daunomycin, which is used to treat leukemia, to double-stranded DNA on silica amine microparticles was investigated by Doughty et al. (111). Daunomycin was found to bind specifically to the attached dsDNA, as excess DNA in solution did not affect binding. This study demonstrated the ability of SHG to detect drug binding and determine the equilibrium constant and Gibbs free energy of binding without labeling of the drug. The same group built on the previous study by investigating the orientation of daunomycin bound to DNA covered microparticles (112). The specificity of daunomycin to a sequence in the dsDNA was used to spatially orient the drug molecules. This study revealed that the interference of the second harmonic fields from a pair of daunomycin molecules bound to DNA can be used to obtain their relative orientation.

Immunoassays

Antibody association to surface-immobilized antigens is extensively used in immunoassays and is conventionally investigated using ELISAs. Though ELISAs are easy to use, disadvantages include

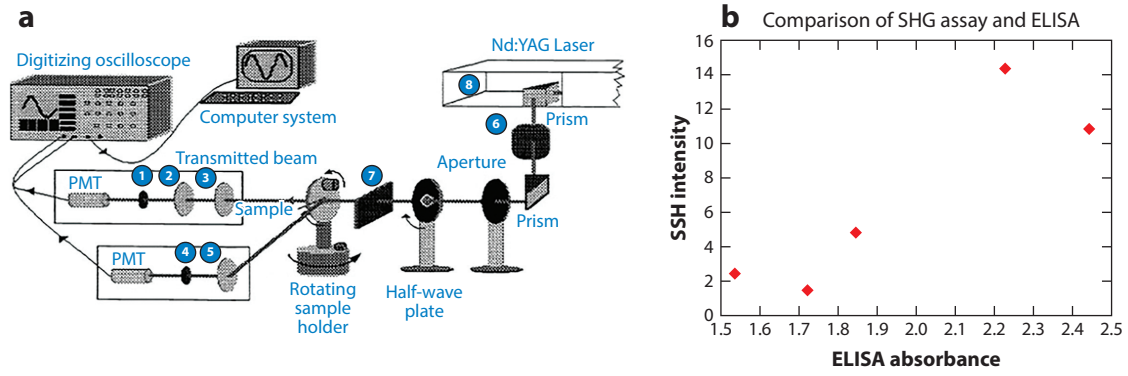

Figure 10

(*a*) Setup of the SHG system used in Reference 113. ❶ and ❹ are 532-nm bandpass filters; ❷, ❸, and ❺ are color glass filters; and ❻ and ❼ are cut-on optical filters. (*b*) Comparison of surface coverage of the anti-BSA IgG antibody using SHG and ELISA from the same ELISA plates, where BSA = 10 μg/ml, 5 ng/well. Figure adapted with permission from Reference 113. Abbreviations: BSA, bovine serum albumin; ELISA, enzyme-linked immunosorbent assay; IgG, immunoglobulin G; PMT, photomultiplier tube; SHG, surface second harmonic generation.

a high risk of contamination and indirect detection using enzymes and colorimetric substrates. As an alternative, SHG could be used as a label-free detection scheme in an ELISA. Yang et al. (113) compared SHG signals obtained from an ELISA plate to the absorbance readings from a sandwich ELISA. Different concentrations of BSA were immobilized in the wells of the ELISA plate before being incubated with different concentrations of anti-BSA antibody. The same ELISA plate was read first before being positioned into the sample holder of the second harmonic setup. This procedure showed that the SH signal was more intense and sensitive and provided the same information as the sandwich ELISA (**Figure 10**). This comparison was further studied when Ditcham et al. (114) examined bovine diarrhea virus against two antibodies by measuring the SH signal from the ELISA plate as well as from glass coverslips covered with antibodies. Like the previous study, it was found that SHG detection in an ELISA has results comparable to those of absorbance-based methods.

An Emerging Technique: Second Harmonic Correlation Spectroscopy

As evident in the previous sections, SHG is capable of detecting the adsorption of proteins, peptides, and small molecules with incredible sensitivity and specificity without the use of an exogenous label. Despite the high sensitivity of SHG, some of the major shortcomings in obtaining binding kinetics and thermodynamics of surface biomolecular interactions in general are the long acquisition times required and large amount of analyte needed to collect a true steady-state binding isotherm. Additionally, if a complete kinetic analysis of the biological surface interaction is desired, both the adsorption and desorption rates must be obtained. To circumvent some of these issues, correlation spectroscopy (CS) was recently applied to SHG.

CS is a well-known statistical analysis method capable of extracting dynamic events within a system by correlating the temporally measured property of the system. CS is routinely used in dynamic light scattering (115–118) and fluorescence (119–123) to evaluate molecular rotational and translational diffusion in bulk solution (124–126), lateral diffusion of biomolecules immobilized at the surface (127, 128), and the binding kinetics of fluorescently labeled molecules at a

surface (123, 129). More recently, CS was combined with Raman spectroscopy (130, 131), coherent X-ray spectroscopy (132–135), and other nonlinear spectroscopies, including SHG (136, 137). However, only a handful of studies used second harmonic correlation spectroscopy (SHCS) (51, 66, 103, 136). Gassin et al. (136) used SHCS to determine the diffusion coefficient of aggregate dye molecules at a surface, and Zhao & Eisenthal (137) looked at the diffusion of long-chain para-substituted amphiphiles using SHCS. All of the SHCS studies are limited to the investigation of molecular diffusion; the authors' group was the first to use this technique for determining the surface binding kinetics of biomolecules.

The authors first demonstrated the utility of SHCS for determining surface interactions of biomolecules by monitoring the intercalation of SBN into a DOPC bilayer (51). No correlation was seen for a DOPC bilayer without SBN, whereas apparent correlated dynamics were observed when SBN intercalated into the DOPC bilayer. Correlation data were fit to the simplified time-dependent correlation function, $G(\tau)$, developed by Starr & Thompson (121) for a reversible biomolecular interaction that is reaction rate limited:

$$G(\tau) = \frac{1}{N_s} \cdot \frac{k_{off}}{k_{on}[c]} \cdot \exp\{-[k_{on}(c) + k_{off}]\tau\}. \quad 10.$$

The above equation allows both the adsorption rate, k_{on}, and desorption rate, k_{off}, to be retrieved from the measured fluctuations in SH intensity for a single analyte concentration $[c]$. N_s is a normalization constant related to the surface density of adsorbed analyte. The SHCS results produced a statistically identical binding affinity to that obtained using a standard steady-state binding isotherm, with the added information of the individual kinetic adsorption and desorption rates. This example of SHCS demonstrates the ease at which the binding kinetics of a simple monovalent surface biomolecular interaction can be accurately determined using less analyte with a shorter collection time. This approach was extended to examine the multivalent proteins CTb and PnA bound to GM_1 doped into a DOPC bilayer using SHCS (66). Multivalent proteins binding to their respective ligands may demonstrate concentration-dependent binding kinetics. Traditional binding isotherms have difficulty examining this property. Alternatively, the ability of SHCS to determine the binding kinetics of a single protein concentration makes it well suited to investigate the concentration-dependent binding kinetics of these multivalent proteins. Correlation data were collected for three bulk CTb concentrations binding to GM_1 doped into a DOPC bilayer, shown in **Figure 11**. **Table 2** shows the kinetic results for both CTb and PnA binding to GM_1. These results illustrate the decrease in binding affinity as the protein concentration is increased, suggesting the presence of a population of high-affinity binders at low concentrations. This study emphasizes the advantage and sensitivity that SHCS offers for examining the binding properties of complex biomolecules at a surface.

PERSPECTIVES AND CONCLUSIONS

SHG is an attractive label-free, highly sensitive, and highly specific method capable of detecting proteins, peptides, and small-molecule adsorption at a surface. The symmetry constraints of SHG afford extreme surface specificity, eliminating contributions from bulk solution molecular diffusion or binding. Additionally, the requirement for a highly ordered net dipole gives SHG the added advantage of being insensitive to randomly ordered nonspecific molecular adsorption at the surface. This is not possible in either of the popular label-free techniques, SPR and QCM. The resonant enhancement of SHG provides incredible sensitivity, down to fg/cm^2, allowing both large proteins and peptides and small-molecule drugs to be detected. The SH output can be tuned to 260–280 nm, where the majority of biomolecules have an electronic transition from π-conjugated systems, giving

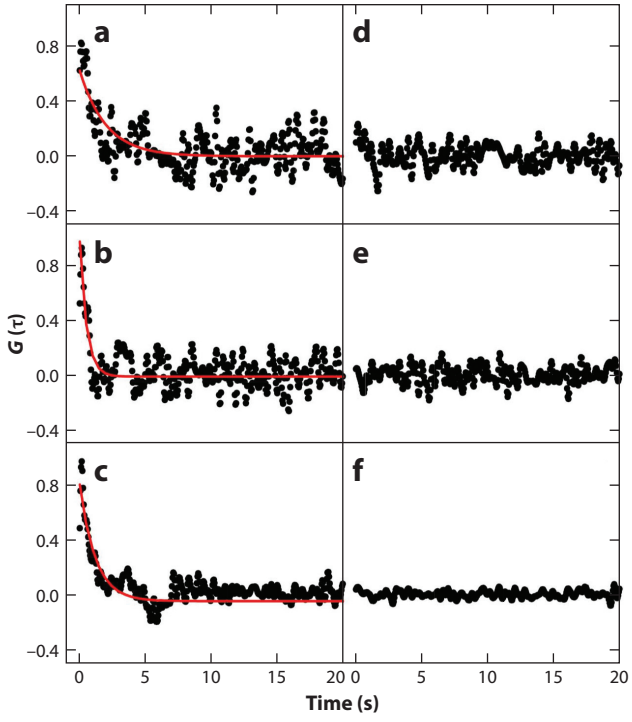

Figure 11

Autocorrelation data for CTb binding to a 1 mol% GM_1 in a DOPC bilayer. Concentrations of CTb are (*a*) 0.5, (*b*) 13, and (*c*) 240 nM, with solid red lines representing fits to Equation 10. Autocorrelation data for CTb binding to a pure DOPC bilayer are shown at (*d*) 0.5, (*e*) 13, and (*f*) 240 nM. Figure adapted with permission from Reference 66. Copyright 2014, American Chemical Society. Abbreviations: CTb, cholera toxin B; DOPC, 1,2-dioleoyl-*sn*-glycero-3-phosphocholine; GM_1, monosialotetrahexosylganglioside.

Table 2 Measured binding kinetics for CTb and PnA binding to a GM_1-doped 1,2-dioleoyl-*sn*-glycero-3-phosphocholine (DOPC) bilayer using second harmonic correlation spectroscopy (SHCS), including the adsorption rate (k_{on}), desorption rate (k_{off}), and equilibrium binding affinity (K_0)

CTb (nM)	k_{on} ($\times 10^8$ M^{-1} s^{-1})	k_{off} ($\times 10^{-5}$ s^{-1})	K_0 ($\times 10^{12}$ M^{-1})
0.5	10 ± 1	3.6 ± 0.5	28 ± 5
13	1.50 ± 0.01	3.2 ± 0.4	4.7 ± 0.7
240	0.035 ± 0.002	2.5 ± 0.2	0.14 ± 0.01
[PnA] (μM)	**k_{on} ($\times 10^5$ M^{-1} s^{-1})**	**k_{off} ($\times 10^{-3}$ s^{-1})**	**K_0 ($\times 10^8$ M^{-1})**
0.43	37 ± 3	1.0 ± 0.2	37 ± 8
3.0	3.9 ± 0.3	2.2 ± 0.2	1.7 ± 0.2
12.2	1.1 ± 0.1	2.7 ± 0.2	0.41 ± 0.05

Abbreviations: CTb, cholera toxin B; PnA, peanut agglutinin.

SHG high sensitivity and versatility. Using the counterpropagating SHG geometry simplifies the detection, as the SH output is separated from the incident beam by a larger degree. Furthermore, counterpropagating SHG allows easy combination with CS with imaging for high-throughput detection. The versatility, high sensitivity, label-free features, and surface specificity of SHG are advantageous properties for biosensor detection and biochemical investigations at interfaces. As the advent of optic technology lowers the cost of high-powered laser systems, the implementation of SHG as a system for the label-free detection of various pharmaceutical/clinical biomolecules will be possible in a more routine fashion.

DISCLOSURE STATEMENT

The authors are not aware of any affiliations, memberships, funding, or financial holdings that might be perceived as affecting the objectivity of this review.

ACKNOWLEDGMENTS

The authors acknowledge the financial support from the National Institutes of Health (R01-GM068120).

LITERATURE CITED

1. Evron T, Peterson SM, Urs NM, Bai Y, Rochelle LK, et al. 2014. G protein and β-arrestin signaling bias at the ghrelin receptor. *J. Biol. Chem.* 289:33442–55
2. Juszczak M, Roszczyk M, Kowalska E, Stempniak B. 2014. The influence of melatonin receptors antagonists, luzindole and 4-phenyl-2-propionamidotetralin (4-P-PDOT), on melatonin-dependent vasopressin and adrenocorticotropic hormone (ACTH) release from the rat hypothalamo-hypophysial system. *In vitro* and *in vivo* studies. *J. Physiol. Pharmacol.* 65:777–84
3. Fukui H, Sueyoshi M, Haritani M, Nakazawa M, Naitoh S, et al. 1995. Natural infection with attaching and effacing Escherichia coli (O 103:H$^-$) in chicks. *Avian Dis.* 39:912–18
4. Negrete OA, Chu D, Aguilar HC, Lee B. 2007. Single amino acid changes in the Nipah and Hendra virus attachment glycoproteins distinguish ephrinB2 from ephrinB3 usage. *J. Virol.* 81:10804–14
5. Sela-Culang I, Kunik V, Ofran Y. 2013. The structural basis of antibody-antigen recognition. *Front. Immunol.* 4:1–13
6. Van Regenmortel MHV. 2014. Specificity, polyspecificity, and heterospecificity of antibody-antigen recognition. *J. Mol. Recognit.* 27:627–39
7. Hall WP, Ngatia SN, Van Duyne RP. 2011. LSPR biosensor signal enhancement using nanoparticle-antibody conjugates. *J. Phys. Chem. C* 115:1410–14
8. Ladd J, Boozer C, Yu Q, Chen S, Homola J, Jiang S. 2004. DNA-directed protein immobilization on mixed self-assembled monolayers via a streptavidin bridge. *Langmuir* 20:8090–95
9. Kudryashov AV, Paxton AH, Ilchenko VS, Aschke L, Washio K, et al. 2014. Interfacing whispering gallery mode microresonators for environmental biosensing. *Proc. SPIE* 8960:89600O
10. Kodoyianni V. 2010. Label-free analysis of biomolecular interactions using SPR imaging. *BioTechniques* 50:32–40
11. Prabowo BA, Chang Y-F, Lee Y-Y, Su L-C, Yu C-J, et al. 2014. Application of an OLED integrated with BEF and giant birefringent optical (GBO) film in a SPR biosensor. *Sens. Actuators B* 198:424–30
12. Janshoff A, Steinem C, Sieber M, Galla H-H. 1996. Specific binding of peanut agglutinin to G_{M1}-doped solid supported lipid bilayers investigated by shear wave resonator measurements. *Eur. Biophys. J.* 25:105–13
13. Ogi H. 2013. Wireless-electrodeless quartz-crystal-microbalance biosensors for studying interactions among biomolecules: a review. *Proc. Jpn. Acad. B* 89:401–17

14. Zhou B, Zhang Z, Zhang Y, Li R, Xiao Q, et al. 2009. Binding of cationic porphyrin to human serum albumin studied using comprehensive spectroscopic methods. *J. Pharm. Sci.* 98:105–13
15. Lu P-P, Meng Z-Y, Wang M-W, Liu T, Wang X, et al. 2007. Interactions between drug and human serum albumin investigated using surface plasmon resonance technology. *Zhongguo Yaolixue Yu Dulixue Zazhi* 21:147–51
16. Heinz TF, Loy MMT, Thompson WA. 1985. Study of Si(111) surfaces by optical second-harmonic generation: reconstruction and surface phase transformation. *Phys. Rev. Lett.* 54:63–66
17. Heskett D, Song KJ, Burns A, Plummer EW, Dai HL. 1986. Coverage dependent phase transition of pyridine on Ag(110) observed by second harmonic generation. *J. Chem. Phys.* 85:7490–92
18. Nguyen TT, Rembert K, Conboy JC. 2009. Label-free detection of drug-membrane association using ultraviolet-visible sum-frequency generation. *J. Am. Chem. Soc.* 131:1401–3
19. Stokes G, Conboy JC. 2014. Measuring selective estrogen receptor modulator (SERM)–membrane interactions with second harmonic generation. *J. Am. Chem. Soc.* 136:1409–17
20. Nguyen TT, Conboy JC. 2011. High-throughput screening of drug-lipid membrane interactions via counter-propagating second harmonic generation imaging. *Anal. Chem.* 83:5979–88
21. Kriech MA, Conboy JC. 2003. Label-free chiral detection of melittin binding to a membrane. *J. Am. Chem. Soc.* 125:1148–49
22. Salafsky JS, Eisenthal KB. 2000. Second harmonic spectroscopy: detection and orientation of molecules at a biomembrane interface. *Chem. Phys. Lett.* 319:435–39
23. Liu Y, Yan ECY, Eisenthal KB. 2001. Effects of bilayer surface charge density on molecular adsorption and transport across liposome bilayers. *Biophys. J.* 80:1004–12
24. Liu Y, Yan ECY, Zhao X, Eisenthal KB. 2001. Surface potential of charged liposomes determined by second harmonic generation. *Langmuir* 17:2063–66
25. Shang X, Liu Y, Yan E, Eisenthal KB. 2001. Effects of counterions on molecular transport across liposome bilayer: probed by second harmonic generation. *J. Phys. Chem. B* 105:12816–22
26. Liu J, Subir M, Nguyen K, Eisenthal KB. 2008. Second harmonic studies of ions crossing liposome membranes in real time. *J. Phys. Chem. B* 112:15263–66
27. Zeng J, Eckenrode HM, Dounce SM, Dai H-L. 2013. Time-resolved molecular transport across living cell membranes. *Biophys. J.* 104:139–45
28. Rao Y, Kwok SJJ, Lombardi J, Turro NJ, Eisenthal KB. 2014. Label-free probe of HIV-1 TAT peptide binding to mimetic membranes. *PNAS* 111:12684–88
29. Salafsky JS, Eisenthal KB. 2000. Protein adsorption at interfaces detected by second harmonic generation. *J. Phys. Chem. B* 104:7752–55
30. Wilhelm MJ, Sheffield JB, Gonella G, Wu Y, Spahr C, et al. 2014. Real-time molecular uptake and membrane-specific transport in living cells by optical microscopy and nonlinear light scattering. *Chem. Phys. Lett.* 605–606:158–63
31. Gomopoulos N, Lutgebaucks C, Sun Q, Macias-Romero C, Roke S. 2013. Label-free second harmonic and hyper Rayleigh scattering with high efficiency. *Opt. Express* 21:815–21
32. Roke S. 2011. Nonlinear spectroscopy of bio-interfaces. *Int. J. Mater. Res.* 102:906–12
33. Roke S, Gonella G. 2012. Nonlinear light scattering and spectroscopy of particles and droplets in liquids. *Annu. Rev. Phys. Chem.* 63:353–78
34. Karam TE, Haber LH. 2014. Molecular adsorption and resonance coupling at the colloidal gold nanoparticle interface. *J. Phys. Chem. C* 118:642–49
35. Nguyen TT, Sly KL, Conboy JC. 2012. Comparison of the energetics of avidin, streptavidin, neutrAvidin, and anti-biotin antibody binding to biotinylated lipid bilayer examined by second-harmonic generation. *Anal. Chem.* 84:201–8
36. Shen YR. 1984. *The Principles of Nonlinear Optics*. Hoboken, NJ: John Wiley & Sons
37. Watry MR, Brown MG, Richmond GL. 2001. Probing molecular structure at liquid surfaces with vibrational sum frequency spectroscopy. *Appl. Spectrosc.* 55:321A–40A
38. Reiser KM, Stoller P, Celliers P, Rubenchik A, Bratton C, Yankelevich D. 2003. Second harmonic generation in collagen. *Proc. SPIE* 5212:149–56

39. Campagnola PJ, Millard AC, Terasaki M, Hoppe PE, Malone CJ, Mohler WA. 2002. Three-dimensional high-resolution second-harmonic generation imaging of endogenous structural proteins in biological tissues. *Biophys. J.* 81:493–508
40. Zhuo Z-Y, Liao C-S, Huang C-H, Yu J-Y, Tzeng Y-Y, et al. 2010. Second harmonic generation imaging—a new method for unraveling molecular information of starch. *J. Struct. Biol.* 171:88–94
41. Eisenthal KB. 1996. Liquid interfaces probed by second-harmonic and sum-frequency spectroscopy. *Chem. Rev.* 96:1343–60
42. Conboy JC, Daschbach JL, Richmond GL. 1994. Total internal reflection second-harmonic generation: probing the alkane water interface. *Appl. Phys. A* 59:623–29
43. Conboy JC, Richmond GL. 1995. Total internal reflection second harmonic generation from the interface between two immiscible electrolyte solutions. *Electrochim. Acta* 40:2881–86
44. Simpson GJ, Westerbuhr SG, Rowlen KL. 2000. Molecular orientation and angular distribution probed by angle-resolved absorbance and second harmonic generation. *Anal. Chem.* 72:887–98
45. Corn RM. 1992. In situ second harmonic generation studies of molecular orientation at electrode surfaces. In *Adsorption of Molecules and Metal Electrodes*, ed. J Lipkowski, P Ross, pp. 391–408. New York: VCH
46. Simpson GJ. 2001. New tools for surface second-harmonic generation. *Appl. Spectrosc.* 55:16A–32A
47. Yamada S, Lee IYS. 1998. Recent progress in analytical SHG spectroscopy. *Anal. Sci.* 14:1045–51
48. Shen YR. 1994. Nonlinear optical studies of surfaces. *Appl. Phys. A* 59:541–43
49. Shen YR. 1989. Optical second harmonic generation at interfaces. *Annu. Rev. Phys. Chem.* 40:327–50
50. Heinz TF, Loy MMT, Thompson WA. 1985. Second-harmonic generation: a probe of symmetry and order in crystalline surfaces. *Springer Ser. Opt. Sci.* 49:311–16
51. Sly KL, Mok S-W, Conboy JC. 2013. Second harmonic correlation spectroscopy: a method for determining surface binding kinetics and thermodynamics. *Anal. Chem.* 85:8429–35
52. Haes AJ, Van Duyne RP. 2002. A nanoscale optical biosensor: sensitivity and selectivity of an approach based on the localized surface plasmon resonance spectroscopy of triangular silver nanoparticles. *J. Am. Chem. Soc.* 124:10596–604
53. Dick B, Gierulski A, Marowsky G, Reider GA. 1985. Determination of the nonlinear optical susceptibility $\chi^{(2)}$ of surface layers by sum and difference frequency generation in reflection and transmission. *Appl. Phys. B* 38:107–16
54. Guyot-Sionnest P, Shen YR, Heinz TF. 1987. Comments on "Determination of the nonlinear optical susceptibility $\chi^{(2)}$ of surface layers" by B. Dick et al. *Appl. Phys. B* 42:237–38
55. Kriech MA, Conboy JC. 2004. Counterpropagating second-harmonic generation: a new technique for the investigation of molecular chirality at surfaces. *J. Opt. Soc. Am. B* 21:1013–22
56. Rao Y, Hong S-Y, Turro NJ, Eisenthal KB. 2011. Molecular orientational distribution at interfaces using second harmonic generation. *J. Phys. Chem. C* 115:11678–83
57. Rao Y, Kwok SJJ, Lombardi J, Turro NJ, Eisenthal KB. 2014. Label-free probe of HIV-1 TAT peptide binding to mimetic membranes. *PNAS* 111:12684–88
58. Matar G, Duboisset J, Benichou E, Bachelier G, Russier-Antoine I, et al. 2010. Second Harmonic Generation, a new approach for analyzing the interfacial properties of a short tryptophan-rich peptide. *Chem. Phys. Lett.* 500:161–66
59. Eckenrode HM, Dai H-L. 2004. Nonlinear optical probe of biopolymer adsorption on colloidal particle surface: poly-L-lysine on polystyrene sulfate microspheres. *Langmuir* 20:9202–9
60. Salafsky JS. 2003. Second-harmonic generation as a probe of conformational change in molecules. *Chem. Phys. Lett.* 381:705–9
61. Moree B, Connell K, Mortensen RB, Liu CT, Benkovic SJ, Salafsky J. 2015. Protein conformational changes are detected and resolved site specifically by second-harmonic generation. *Biophys. J.* 109:806–15
62. Moree B, Yin G, Lázaro DF, Munari F, Strohäker T, et al. 2015. Small molecules detected by second-harmonic generation modulate the conformation of monomeric α-synuclein and reduce its aggregation in cells. *J. Biol. Chem.* 290:27582–93
63. Salafsky JS, Cohen B. 2008. A second-harmonic-active unnatural amino acid as a structural probe of biomolecules on surfaces. *J. Phys. Chem. B* 112:15103–7
64. Zhao S, Walker DS, Reichert WM. 1993. Cooperativity in the binding of avidin to biotin-lipid-doped Langmuir-Blodgett films. *Langmuir* 9:3166–73

65. Saad JS, Loeliger E, Luncsford P, Liriano M, Tai J, et al. 2007. Point mutations in the HIV-1 matrix protein turn off the myristyl switch. *J. Mol. Biol.* 366:574–85
66. Sly KL, Conboy JC. 2014. Determination of multivalent protein–ligand binding kinetics by second-harmonic correlation spectroscopy. *Anal. Chem.* 86:11045–54
67. Sakamaki K, Sawada K, Koshimizu U, Nishimune Y. 1989. Identification of peanut agglutinin receptors on mouse testicular germ cells. *Biol. Reprod.* 41:1097–102
68. Devlin TM, ed. 1997. *Textbook of Biochemistry with Clinical Correlations*. Hoboken, NJ: Wiley. 4th ed.
69. Giordmaine JA, Rentzepis PM. 1967. Correlation of optical activity and nonlinear polarizability. *J. Chim. Phys.* 64:215–21
70. Simon HJ, Bloembergen N. 1968. Second-harmonic light generation in crystals with natural optical activity. *Phys. Rev.* 171:1104–14
71. Verbiest T, Kauranen M, Van Elshocht S, Persoons A. 1999. Optical susceptibilities of chiral systems and chiral thin films. *Nonlin. Opt.* 22:155–60
72. Persoons A, Kauranen M, Van Elshocht S, Verbiest T, Ma L, et al. 1998. Chiral effects in second-order nonlinear optics. *Mol. Cryst. Liq. Cryst. Sci. Technol. A* 315:395–400
73. Kauranen M, Verbiest T, Maki JJ, Persoons A. 1996. Chirality effects in second-order nonlinear optics. In *NATO Advanced Research Workshop on Photoactive Organic Materials: Science and Applications*, ed. F Kajzar, VM Agranovich, CY-C Lee, pp. 129–44. Dordrecht, Neth.: Kluwer
74. Hicks JM, Petralli-Mallow T. 1999. Nonlinear optics of chiral surface systems. *Appl. Phys. B* 68:589–93
75. Petralli-Mallow T, Wong TM, Byers JD, Yee HI, Hicks JM. 1993. Circular dichroism spectroscopy at interfaces: a surface second harmonic generation study. *J. Phys. Chem.* 97:1383–88
76. Hicks JM, Petralli-Mallow T, Byers JD. 1994. Consequences of chirality in second-order non-linear spectroscopy at surfaces. *Faraday Discuss. Pap.* 99:341–57
77. Byers JD, Hicks JM. 1994. Electronic spectral effects on chiral surface second harmonic generation. *Chem. Phys. Lett.* 231:216–24
78. Byers JD, Yee HI, Hicks JM. 1994. A second harmonic generation analog of optical rotatory dispersion for the study of chiral monolayers. *J. Chem. Phys.* 101:6233–41
79. Byers JD, Yee HI, Petralli-Mallow T, Hicks JM. 1994. Second-harmonic generation circular-dichroism spectroscopy from chiral monolayers. *Phys. Rev. B* 49:14643–47
80. Yamada T, Haruyama Y, Kasai K, Terui T, Tanaka S, et al. 2012. Orientation of a bacteriorhodopsin thin film deposited by dip coating technique and its chiral SHG as studied by SHG interference technique. *Chem. Phys. Lett.* 530:113–19
81. Tao Y, Cheben P, Aldea-Nunzi G, Rao Bobbara S, Nunzi J-M, et al. 2013. Second harmonic generation of chiral-modified silver nanoparticles. *Proc. SPIE* 8915:891513
82. Kriech MA, Conboy JC. 2005. Using the intrinsic chirality of a molecule as a label-free probe to detect molecular adsorption to a surface by second harmonic generation. *Appl. Spectrosc.* 59:746–53
83. Dawson CR, Drake AF, Helliwell J, Hider RC. 1978. The interaction of bee melittin with lipid bilayer membranes. *Biochim. Biophys. Acta* 510:75–86
84. Frey S, Tamm LK. 1991. Orientation of melittin in phospholipid bilayers. A polarized attenuated total reflection infrared study. *Biophys. J.* 60:922–30
85. Buckley P, Edison AS, Kemple MD, Prendergast FG. 1993. $^{13}C^{\alpha}$-NMR assignments of melittin in methanol and chemical shift correlations with secondary structure. *J. Biomol. NMR* 3:639–52
86. Lam YH, Wassall SR, Morton CJ, Smith R, Separovic F. 2001. Solid-state NMR structure determination of melittin in a lipid environment. *Biophys. J.* 81:2752–61
87. Yang L, Harroun TA, Weiss TM, Ding L, Huang HW. 2001. Barrel-stave model or toroidal model? A case study on melittin pores. *Biophys. J.* 81:1475–85
88. Kubota S, Yang JT. 1986. Conformation and aggregation of melittin: effect of pH and concentration of sodium dodecyl sulfate. *Biopolymers* 25:1493–504
89. Maulet Y, Cox JA. 1983. Structural changes in melittin and calmodulin upon complex formation and their modulation by calcium. *Biochemistry* 22:5680–86
90. Terwilling TC, Eisenberg D. 1982. The structure of melittin: structure determination and partial refinement. *J. Biol. Chem.* 257:6010–15

91. Dempsey CE, Watts A. 1987. A deuterium and phosphorus-31 nuclear magnetic resonance study of the interaction of melittin with dimyristoylphosphatidylcholine bilayers and the effects of contaminating phospholipase A2. *Biochemistry* 26:5803–11
92. Sharifian M, Wilhelm MJ, Dai H-L. 2016. Label-free optical method for quantifying molecular transport across cellular membranes in vitro. *J. Phys. Chem. Lett.* 7:3406–11
93. Mitchell SA. 2009. Indole adsorption to a lipid monolayer studied by optical second harmonic generation. *J. Phys. Chem. B* 113:10693–707
94. Hellwarth R, Christensen P. 1974. Nonlinear optical microscopic examination of structure in polycrystalline zinc selenide. *Opt. Commun.* 12:318–22
95. Motreff A, Raffy G, Del Guerzo A, Belin C, Dussauze M, et al. 2010. Chemisorption of fluorous copper(II)-carboxylate complexes on SiO_2 surfaces: versatile binding layers applied to the preparation of porphyrin monolayers. *Chem. Commun.* 46:2617–19
96. Iwamoto M, Manaka T. 2011. Probing and modeling of carrier motion in organic devices by optical second harmonic generation. *Thin Solid Films* 519:961–63
97. Kriech MA, Conboy JC. 2005. Imaging chirality with surface second harmonic generation microscopy. *J. Am. Chem. Soc.* 127:2834–35
98. Macias-Romero C, Didier MEP, Jourdain P, Marquet P, Magistretti P, et al. 2014. High throughput second harmonic imaging for label-free biological applications. *Opt. Express* 22:31102
99. Bouevitch O, Lewis A, Pinevsky I, Wuskell JP, Loew LM. 1993. Probing membrane potential with nonlinear optics. *Biophys. J.* 65:672–79
100. Ben-Oren I, Peleg G, Lewis A, Minke B, Loew L. 1996. Infrared nonlinear optical measurements of membrane potential in photoreceptor cells. *Biophys. J.* 71:1616–20
101. Moreaux L, Sandre O, Blanchard-Desce M, Mertz J. 2000. Membrane imaging by simultaneous second-harmonic generation and two-photon microscopy. *Opt. Lett.* 25:320–22
102. Srivastava A, Eisenthal KB. 1998. Kinetics of molecular transport across a liposome bilayer. *Chem. Phys. Lett.* 292:345–51
103. Yan ECY, Eisenthal KB. 2000. Effect of cholesterol on molecular transport of organic cations across liposome bilayers probed by second harmonic generation. *Biophys. J.* 79:898–903
104. Peleg G, Lewis A, Linial M, Loew LM. 1999. Nonlinear optical measurement of membrane potential around single molecules at selected cellular sites. *PNAS* 96:6700–4
105. Goldsmith PF. 1998. *Quasioptical Systems: Gaussian Beam Quasioptical Propagation and Applications*. Hoboken, NJ: Wiley/IEEE
106. Troiano JM, Kuech TR, Vartanian AM, Torelli MD, Sen A, et al. 2016. On electronic and charge interference in second harmonic generation responses from gold metal nanoparticles at supported lipid bilayers. *J. Phys. Chem. C* 120:20659–67
107. Perrenoud-Rinuy J, Brevet P-F, Girault HH. 2002. Second harmonic generation study of myoglobin and hemoglobin and their protoporphyrin IX chromophore at the water/1,2-dichloroethane interface. *Phys. Chem. Chem. Phys.* 4:4774–81
108. Kumal RR, Abu-Laban M, Landry CR, Kruger B, Zhang Z, et al. 2016. Plasmon-enhanced photocleaving dynamics in colloidal microRNA-functionalized silver nanoparticles monitored with second harmonic generation. *Langmuir* 32:10394–401
109. Walter SR, Geiger FM. 2010. DNA on stage: showcasing oligonucleotides at surfaces and interfaces with second harmonic and vibrational sum frequency generation. *J. Phys. Chem. Lett.* 1:9–15
110. Doughty B, Kazer SW, Eisenthal KB. 2011. Binding and cleavage of DNA with the restriction enzyme ecor1 using time-resolved second harmonic generation. *PNAS* 108:19979–84
111. Doughty B, Rao Y, Kazer SW, Kwok SJJ, Turro NJ, Eisenthal KB. 2013. Binding of the anti-cancer drug daunomycin to DNA probed by second harmonic generation. *J. Phys. Chem. B* 117:15285–89
112. Doughty B, Rao Y, Kazer SW, Kwok SJJ, Turro NJ, Eisenthal KB. 2013. Probing the relative orientation of molecules bound to DNA through controlled interference using second-harmonic generation. *PNAS* 110:5756–58
113. Yang L, McStay D, Quinn PJ. 1996. Surface second harmonic generation (SSHG): a new scheme for immunoassay. *Proc. SPIE* 2676:290–96

114. Ditcham WGF, Al-Obaidi AHR, McStay D, Mottram TT, Brownlie J, Thompson I. 2001. An immunosensor with potential for the detection of viral antigens in body fluids, based on surface second harmonic generation. *Biosens. Bioelectron.* 16:221–24
115. Pecora R. 1964. Doppler shifts in light scattering from pure liquids and polymer solutions. *J. Chem. Phys.* 40:1604–14
116. Pecora R, ed. 1985. *Dynamic Light Scattering: Applications of Photon Correlation Spectroscopy*. New York: Plenum
117. Cummins HZ, Pike ER, eds. 1973. *Photon Correlation and Light Beating Spectroscopy*, Vol. 3. New York: Plenum
118. Cummins HZ, Knable N, Yeh Y. 1964. Observation of diffusion broadening of Rayleigh scattered light. *Phys. Rev. Lett.* 12:150–53
119. Bismuto E, Gratton E, Lamb DC. 2001. Dynamics of ANS binding to tuna apomyoglobin measured with fluorescence correlation spectroscopy. *Biophys. J.* 81:3510–21
120. Chattopadhyay K, Saffarian S, Elson EL, Frieden C. 2005. Measuring unfolding of proteins in the presence of denaturant using fluorescence correlation spectroscopy. *Biophys. J.* 88:1413–22
121. Starr TE, Thompson NL. 2001. Total internal reflection with fluorescence correlation spectroscopy: combined surface reaction and solution diffusion. *Biophys. J.* 80:1575–84
122. Fahey PF, Koppel DE, Barak LS, Wolf DE, Elson EL, Webb WW. 1977. Lateral diffusion in planar lipid bilayers. *Science* 195:305–6
123. Hansen RL, Harris JM. 1998. Measuring reversible adsorption kinetics of small molecules at solid/liquid interfaces by total internal reflection fluorescence correlation spectroscopy. *Anal. Chem.* 70:4247–56
124. Kuttner YY, Kozer N, Segal E, Schreiber G, Haran G. 2005. Separating the contribution of translational and rotational diffusion to protein association. *J. Am. Chem. Soc.* 127:15138–44
125. Rodriguez-Maldonado L, Fernandez-Nieves A, Fernandez-Barbero A. 2005. Dynamic light scattering from high molecular weight poly-L-lysine molecules. *Colloids Surf. A* 270–271:335–39
126. Nordmeier E. 1993. Static and dynamic light-scattering solution behavior of pullulan and dextran in comparison. *J. Phys. Chem.* 97:5770–85
127. Kelly CV, Wakefield DL, Holowka DA, Craighead HG, Baird BA. 2014. Near-field fluorescence cross-correlation spectroscopy on planar membranes. *ACS Nano* 8:7392–404
128. Macháň R, Jurkiewicz P, Olżyńska A, Olšinová M, Cebecauer M, et al. 2014. Peripheral and integral membrane binding of peptides characterized by time-dependent fluorescence shifts: focus on antimicrobial peptide LAH_4. *Langmuir* 30:6171–79
129. Thompson NL, Axelrod D. 1983. Immunoglobulin surface-binding kinetics studied by total internal reflection with fluorescence correlation spectroscopy. *Biophys. J.* 43:103–14
130. Asiala SM, Schultz ZD. 2014. Surface enhanced Raman correlation spectroscopy of particles in solution. *Anal. Chem.* 86:2625–32
131. Brun N, Ponçot M, Bourson P. 2013. Raman correlation spectroscopy: a method studying physical properties of polystyrene by the means of multivariate analysis. *Chemom. Intell. Lab. Syst.* 128:77–82
132. Riese DO, Vos WL, Wegdam GH, Poelwijk FJ, Abernathy DL, Grübel G. 2000. Photon correlation spectroscopy: X rays versus visible light. *Phys. Rev. E* 61:1676–80
133. Dierker SB, Pindak R, Fleming RM, Robinson IK, Berman L. 1995. X-ray photon corelation spectroscopy study of Brownian motion of gold colloids in glycerol. *Phys. Rev. Lett.* 75:449–52
134. Eisebitt S, Lörgen M, Eberhardt W, Lüning J, Stöhr J, et al. 2003. Polarization effects in coherent scattering from magnetic specimen: implications for x-ray holography, lensless imaging, and correlation spectroscopy. *Phys. Rev. B* 68:104419
135. Grübel G, Abernathy DL, Riese DO, Vos WL, Wegdam GH. 2000. Dynamics of dense, charge-stabilized suspensions of colloidal silica studied by correlation spectroscopy with coherent X-rays. *J. Appl. Crystallogr.* 33:424–27
136. Gassin P-M, Martin-Gassin G, Benichou E, Brevet P-F. 2014. Tracking molecular aggregates at a liquid interface by nonlinear correlation spectroscopy. *J. Phys. Chem. C* 118:1135–41
137. Zhao X, Eisenthal KB. 1995. Monolayer orientational fluctuations and a new phase transition at the air water interface detected by second harmonic generation. *J. Chem. Phys.* 102:5818–26

138. Frostell-Karlsson Å, Remaeus A, Roos H, Andersson K, Borg P, et al. 2000. Biosensor analysis of the interaction between immobilized human serum albumin and drug compounds for prediction of human serum albumin binding levels. *J. Med. Chem*. 43:1986–92
139. Murtaza R, Jackman HL, Alexander B, Lleshi-Tali A, Winnie AP, Igic R. 2001. Simultaneous determination of mepivacaine, tetracaine, and *p*-butylaminobenzoic acid by high-performance liquid chromatography. *J. Pharmacol. Toxicol. Methods* 46:131–36
140. Shi J, Yang T, Kataoka S, Zhang Y, Diaz AJ, Cremer PS. 2007. GM_1 clustering inhibits cholera toxin binding in supported phospholipid membranes. *J. Am. Chem. Soc.* 129:5954–61
141. Svennerholm A-M, Wiklund G. 1983. Rapid GM1-enzyme-linked immunosorbant assay with visual reading for identification of *Escherichia coli* heat-labile enterotoxin. *J. Clin. Microbiol.* 17:596–600
142. Vornholt W, Hartmann M, Keusgen M. 2007. SPR studies of carbohydrate–lectin interactions as useful tool for screening on lectin sources. *Biosens. Bioelectron.* 22:2983–88
143. Jung H, Yang T, Lasagna MD, Shi J, Reinhart GD, Cremer PS. 2008. Impact of hapten presentation on antibody binding at lipid membrane interfaces. *Biophys. J.* 94:3094–103
144. Nielsen UB, Geierstanger BH. 2004. Multiplexed sandwich assays in microarray format. *J. Immunol. Methods* 290:107–20